Influence of a series of pyridine ligands on the structure and photophysical properties of Cd(II) complexes†

Daniel Ejarque, [a] Teresa Calvet, [b] Mercè Font-Bardia [c] and Josefina Pons [*a]

[a] Departament de Química, Universitat Autònoma de Barcelona ,08193 Barcelona, Spain; E-mail: josefina.pons@uab.es

[b] Departament de Mineralogia, Petrologia i Geologia Aplicada, Universitat de Barcelona, Martí i Franquès s/n, 08028 Barcelona, Spain

[c] Unitat de Difracció de Raig-X, Centres Científics i Tecnològics de la Universitat de Barcelona (CCiTUB), Universitat de Barcelona, Solé i Sabarís, 1-3, 08028 Barcelona, Spain

Abstract

Among the group 12 metal ions, the Cd(II) ion presents an ionic radius comparable to that of Hg(II), while its electronegativity resembles that of Zn(II). Thus, these characteristics make it a suitable candidate for the synthesis of fluorescent coordination complexes given that it tends to maximize the chelation enhanced effect (CHEF), while its electronegativity helps to prevent the quenching of fluorescence generated by the heavy atom effect. Accordingly, herein, we performed a systematic study using Cd(II) compounds bearing α-acetamidocinnamic acid (HACA) and different N-, N^N- and N^N^N-pyridine ligands (dPy), namely pyridine (py) (1), 3-phenylpyridine (3-phpy) (2), 2,2′-bipyridine (2,2′-bipy) (3), 1,10-phenantroline (1,10-phen) (4) and 2,2′:6′,2″-terpyridine (terpy) (5). The elucidation of their crystal structures revealed the formation of one coordination polymer (1), one dimer (3) and three monomers (2, 4, and 5). All the synthesized compounds were characterized via analytical and spectroscopic techniques, and their molecular and supramolecular structures were discussed. The photophysical properties of 1–5 in MeOH were studied and their quantum yields (Φ) were calculated, revealing an enhancement in the Φ value of the complexes generated by the CHEF of dPy.

1. Introduction

Recently, the design of coordination compounds for specific applications has attracted increasing attention owing to their mild reaction conditions, versatility and diverse applications.1–7 Furthermore, the understanding of their structure–property relationship has allowed the rational selection of appropriate metal nodes and organic ligands for the design of monomers, dimers, and coordination polymers (CPs), taking advantage of their structural mouldability.8,9

Accordingly, the synthesis of discrete coordination complexes with fluorescent properties in solution has been widely reported, benefiting from their better solvent processability compared with CPs.10,11 Moreover, their inherent capability to rigidify the precursor organic ligands through coordination with metal ions provides an enhancement in the resulting photophysical properties, benefiting from the chelation enhanced effect (CHEF) thus avoiding energy loss through bond vibrations or photoinduced electron transfer (PET) processes.12–15 However, coordination complexes also present some drawbacks, which can cause a reduction in the fluorescence efficiency (quantum yield, Φ) such as the heavy atom and steric crowding effect. The former is related to the large spin–orbit coupling constant (ζ) of heavy atoms, which promotes intersystem crossing to the triplet state, favoring the quenching process.16,17 Nonetheless, the degree of covalency in coordination bonds also plays an important role, avoiding the heavy atom effect in the case of poorly covalent complexes such as lanthanide complexes.18 Besides, the steric crowding effect is related to the elongation of coordination bonds in complexes with small ionic radii, which hinders CHEF, and therefore reduces the fluorescence efficiency through PET mechanisms.19,20

In this scenario, group 12 metal ions emerge as good candidates for the synthesis of efficient fluorescent complexes owing to the absence of potential quenching processes derived from d-d transitions and their zero-crystal field stabilization energy (CFSE), which offer a wide variety of possible geometries, making them ideal building blocks.21,22 Among them, Cd(II) stands out as the most promising metal ion in this group given that it presents a similar ionic radius to that of Hg(II), but its electronegativity resembles that of Zn(II).23,24 These characteristics permit it to maximize CHEF, while preventing the heavy atom effect. Therefore, several examples of Cd(II) complexes containing pyridine ligands (dPy) with enhanced Φ values produced by the maximization of CHEF and the prevention of heavy

atom effect have been reported in the literature.25,26 Additionally, the size of the Cd(II) metal core allows compounds with diverse coordination numbers to be obtained, usually between four and eight, thus allowing their structural modulation mainly based on steric requirements.27,28

In previous contributions, our group studied the reactivity of α-acetamidocinnamic acid (HACA) towards Zn(II) and Cd(II), obtaining monomeric complexes.29 In addition, the incorporation of 4-phenylpyridine resulted in the formation of monomeric, dimeric, trimeric and polymeric compounds, depending on the synthetic conditions.29,30 Recently, we studied the effect of adding different N,N^N, and N^N^N dPy ligands on the structure and photophysical properties of Zn(II) compounds bearing ACA, obtaining monomeric or polymeric complexes depending on the coordination of the acetamide moiety of ACA. In addition, the photophysical properties of these compounds were analyzed, observing the dominant impact of steric crowding over CHEF as the size of the coordinated dPy increased, which was reflected in the Φ values.31

Following this study and aiming to prove the suitability of Cd(II) complexes as efficient fluorescent compounds, herein, we studied the impact of adding a series of N-donors (pyridine, py; 3-phenylpyridine, and 3-phpy), N^N-donors (2,2′ -bipyridine, 2,2′ -bipy; 1,10-phenanthroline, and 1,10- phen) and N^N^N-donor (2,2′ :6′ ,2″ -terpyridine, terpy) ligands on the structure and photophysical properties of Cd(II) complexes incorporating ACA in their structure. The increasing denticity of the selected dPy was expected to favor the formation of chelate coordination modes, maximizing CHEF. Moreover, the quenching effect produced by steric crowding was also prevented owing to the bigger ionic radii of Cd(II) (0.95 Å) compared with that of Zn(II) (0.74 Å).23

Within this frame, the reactions of Cd(OAc)2·2H2O, HACA and the mentioned dPy ligands were performed, resulting in the formation of one coordination polymer (CP), one dimeric and three monomeric complexes, as follows: [CdIJμ-O,O′ - ACA)IJACA)IJpy)]n (1), [Cd(ACA)2(3-phpy)2(H2O)2]·2H2O (2), [Cd(ACA)2(2,2′ -bipy)]2 • 2MeOH (3), [Cd(ACA)2(1,10-phen)]·3EtOH (4) and [Cd(ACA)2(terpy)]·2DMF (5) (Scheme 1). These compounds were characterized via analytical and spectroscopic techniques, and their crystal structures elucidated. We further investigated their photophysical properties in MeOH solution and calculated their Φ values, which are related to the CHEF of the pyridines.

2. Results and discussion

Synthesis and characterization

Compounds 1 – 5 were prepared via the combination of Cd(OAc)2 • 2H2O, HACA and the corresponding dPy (dPy = py (1), 3-phpy (2), 2,2′ -bipy (3), 1,10-phen • H2O (4), and terpy (5)) in a 1 :2:2 (1), 1:2:3 (2) or 1 : 2 : 1 (3–5) molar ratio, using EtOH at room temperature (RT). The corresponding crystals suitable for X-ray crystallographic analysis were obtained by keeping the mother liquor sealed in a fridge (1), and by recrystallization of the obtained solid in MeOH (3), EtOH (2 and 4) or DMF (5), at RT. Further details of the synthetic methodologies and the procedure for obtaining single crystals are provided in the Experimental Section.

Compounds 1 – 5 were prepared via the combination of Cd(OAc)2 • 2H2O, HACA and the corresponding dPy (dPy = py (1), 3-phpy (2), 2,2′ -bipy (3), 1,10-phen • H2O (4), and terpy (5))

in a 1 :2:2 (1), 1:2:3 (2) or 1 : 2 : 1 (3–5) molar ratio, using EtOH at room temperature (RT). The corresponding crystals suitable for X-ray crystallographic analysis were obtained by keeping the mother liquor sealed in a fridge (1), and by recrystallization of the obtained solid in MeOH (3), EtOH (2 and 4) or DMF (5), at RT. Further details of the synthetic methodologies and the procedure for obtaining single crystals are provided in the Experimental Section.

The EA of 1–5 agree with their proposed formula (Scheme 1). The FTIR-ATR spectra show the absence of a broad band between 2704 and 2405 cm−1, which corresponds to ν(O–H)HACA, indicating that HACA is deprotonated in the five complexes. The spectra show the characteristic bands in the range of 1559–1514 cm−1 for νas(COO) and 1406–1389 cm−1 for νs(COO) (ESI:† Fig. S1–S5). The difference between these bands [Δ = νas(COO) − νs(COO)] is 133 (1), 170 (2), 125 and 144 (3), 123 (4) and 130 (5) cm−1, suggesting chelate (1 and 3 – 5), pseudo-bridged (2),32,33 and bridged and chelate (3) coordination modes of the carboxylate groups.32,34 All the Δ values agree with the data obtained from the crystal structures. In addition, the NH and C O groups of ACA, and the signals of the aromatic rings, were also identified.35

The presence of solvent molecules allowed further identification of some specific bands at 3638, 3299 (2), 3365 (3) and 3388 (4) cm−1, corresponding to ν(O–H) from the water or alcohol solvent. In the case of 2, the sharp peak at 3638 cm−1 suggests the coordination of water molecules to the Cd(II) center, which may promote strong hydrogen bonds with the carboxylate groups from ACA, affecting its Δ value.32 Similarly, the presence of an additional ν(C O) signal at 1703 cm−1 in 5 suggests the presence of DMF.34,35 The 1H, 13C{1H} and DEPT-135 NMR spectra of 1–5 were recorded in DMSO-d6 solution. The 1H NMR spectra show the characteristic signal of the NH moiety between 9.18 and 9.09 ppm. In addition, the aromatic protons from ACA together with the hydrogen atom from the alkene group appear between 7.51 and 7.22 ppm. The protons corresponding to the dPy ligands appeared between 9.19 and 7.41 ppm and the methyl protons from ACA between 1.96 and 1.93 ppm (ESI:† Fig. S6–S10). Noteworthily, the spectrum of 5 at 300 K shows broad signals of the terpy ligand, which upon an increase in temperature from 300 to 340 K, exhibited improved resolution (ESI:† Fig. S11). This behavior is attributed to the presence of planar interactions between the terpy ligands.36,37 Overall, the 1H NMR spectra of 1 and 3–5 indicate a 2ACA : 1dPy molar ratio, while that in 2 is 1ACA : 1dPy.

The 13C{1H} NMR spectra of the five complexes display a band that can be assigned to the carbon atom from the carbonyl group between 171.54–170.52 ppm followed by the carbon atom from the carboxylate groups, which appear between 168.51 and 167.96 ppm. The carbon atoms from the dPy ligands are observed between 150.56 and 121.95 ppm, while the signals corresponding to the alkene group of ACA were observed at 135.51–135.23 ppm and 128.25–127.87 ppm. Moreover, the aromatic carbon atoms from ACA were located between 129.90–128.21 ppm and the methyl carbon atoms between 23.22–23.05 ppm (ESI:† Fig. S12–S16).35

The coordination of the ligands to the Zn(II) cores in solution was verified in 3–5 by the chemical shift of o-H (3: 8.81; 4: 9.19; 5: 8.99 ppm) of dPy and the carboxylate signals of ACA (3: 168.38; 4: 168.14; and 5: 167.96 ppm), which is consistent with their coordination compared with that of HACA (162.70 ppm) and the free dPy ligands (2,2′ -bipy: 8.55 ppm; 1,10-phen: 8.80; and terpy: 8.55 ppm) in DMSO-d6. Besides, the 1H NMR spectra of 1 and 2 do not show an apparent chemical shift for the dPy signals in comparison with that of the free py and 3-phpy, proving that they are not coordinated in this solvent. Therefore, 1H, 13C{1H} and DEPT-135 experiments in MeOH-d4 for 1 and 2 were carried

out, showing that in these solvents, both ACA (1: 172.95 and 2: 172.87 ppm) and dPy (1: 8.61 and 2: 8.81 and 8.52 ppm) are coordinated and display chemical shifts with respect to the free HACA (168.19 ppm) and dPy (py: 8.33 and 3-phpy: 8.75 and 8.48 ppm) (ESI:† Fig. S17–S20). Finally, the 13C{1H} NMR spectrum of 1 in MeOH-d4 suggests that after being dissolved, the coordination bond of the carbonyl group is broken, forming monomeric units.

Crystal structure analysis

The evaluation of the geometry of the Cd(II) cores in compounds 1–5 was performed using version 2.1 of the SHAPE software,38 which is based on the low continuous shape measure (CShM) value S,39 giving information on the deviation of the desired polyhedron from the selected ideal geometry. In addition, the average twist angle (ata)40,41 values were also calculated using the .cif files.

Crystal and extended structure of 1. Compound 1 crystallizes in the monoclinic P21/n space group. It consists of a Cd(II) polymeric structure expanded in a zig-zag shape through the b axis by a ligand bridge involving one of the ACA ligands via carboxylate and carbonyl groups (Fig. 1a). Noteworthy, compound 1 is isostructural to a CP with the formula [Zn(μ -O,O′ -ACA)(ACA)(py)]n previously obtained by our group.31 Furthermore, the same behavior of the carbonyl group was also observed in another Zn(II) CP bearing 4-phenylpyridine.30 The formation of these polymeric chains is attributed to the low size of the pyridine ligand, which allows the entry of the carbonyl group in the coordination sphere of the metallic centers. The metal centers present a [CdO5N] core composed of two asymmetrically bidentate chelate (μ1-η2) ACA, one py ligand and one carbonyl group, generating a distorted trigonal prismatic geometry (S = 6.631). Additionally, the bond lengths and bond angles oscillate between 2.2502(14)– 2.4639(13) Å and 55.98(4)–147.71(5)°, presenting similar values to that of other Cd(II) CPs with coordinated carboxylate and carbonyl moieties combined with dPy (ESI:† Table S1).42,43

Compound 1 presents different intramolecular interactions, which stabilize the polymeric array. These are mainly based on the N–H···OC O synthon via contiguous amide groups combined with π···π stacking between ACA and the py aromatic rings and additional C–H···O associations, all supporting the polymeric structure (Fig. 1b and ESI:† Table S1). The intermolecular interactions of 1 form 2D layers through the (220) plane (Fig. 1c), which are based on the reciprocal N(1)–H(1)···O(2)COO synthon combined with C–H···π associations involving nearby ACA aromatic rings (Fig. 1d).

Crystal and extended structure of 2. Compound 2 crystallizes in the monoclinic P21/c space group. It consists of a Cd(II) monomeric structure with a [CdO4N2] core composed of two monodentate (μ1-η1) ACA ligands, two twisted 3-phpy (41.02°), and two water molecules, where all of them are in a trans configuration. The geometry of the Cd(II) center displays an octahedral geometry (S = 0.054) (Fig. 2a). The bond lengths and bond angles oscillate between 2.2804(9)– 2.3311(10) Å and 87.54(3)–180°, presenting similar values to that of other monomeric hexacoordinated Cd(II) compounds bearing μ1-η1 coordinated carboxylate moieties, dPy and water molecules (ESI:† Table S2).44,45 Additionally, its crystal structure contains two occluded water molecules.

Compound 2 displays a strong intramolecular H-bond between the coordinated water molecules and non- coordinated oxygen atoms from the carboxylate groups of ACA (Fig. 2a). Their intermolecular interactions are based on the reciprocal N–H···OCOO synthon combined with a pattern of H-bonds between the coordinated and non-coordinated water molecules, which are joined by consecutive H-bonds between their hydroxyl groups. Additionally, the occluded water molecules are also associated with nearby monomeric units by an H-bond involving the carbonyl oxygen atom from an ACA. These interactions expand the structure through the ac plane (Fig. 2b). Finally, a C–H···O interaction between one m-H from ACA and the coordinated water molecules, and a C–H···π association between contiguous 3-phpy ligands expand the structure along the [011] direction, which in combination with the expansion along the ac plane forms a 3D network (Fig. 2c and ESI:† Table S2).

Crystal and extended structure of 3. Compound 3 crystallizes in the triclinic $P\bar{1}$ space group. It consists of a dimeric structure with a [CdO5N2] core composed of four ACA and two twisted 2,2′-bipy (16.95°) ligands. Two of the ACA ligands exhibit both asymmetric bridged and chelate coordination modes (μ2-η2:η1), joining the Cd(II) centers. Moreover, the remaining ACA and the 2,2′-bipy ligands display μ1-η2 coordination modes (Fig. 3a). The metal core adopts a capped trigonal prismatic geometry (S = 5.477), where the capped position is occupied by one of the carboxylate oxygen atoms (O1). The bond lengths and angles are in the range of 2.3162(16)–2.4423(14) Å and 54.58(4)–142.45(5)° (ESI:† Table S3), which are similar to that of other reported hepta-coordinated Cd(II) compounds containing carboxylate ligands and 2,2′-bipy.46–48 Additionally, its crystal structure presents two occluded MeOH molecules.

The dimeric structure contains intramolecular N–H···OCOO interactions between the ACA ligands, while the 2,2′ -bipy units interact with the ACA ligands via C–H···O associations, both stabilizing the dimeric array (Fig. 3b). Their intermolecular interactions are driven by the reciprocal N– H···OCOO synthon combined with additional C–H···O between the 2,2′ bipy and ACA ligands, which extend the structure through the a direction (Fig. 3c). In addition, these chains generate an accessible volume of 9.10 Å3 (0.6% of the unit cell volume, calculated using the probe radius of 1.2 Å),49 where the MeOH molecules join the dimeric arrays by H-bonds and C–H···O interactions, involving both ACA and 2,2'-bipy ligands supported by additional C–H···π associations. These group of interactions expand the structure along the bc plane (Fig. 3d), which in combination with the a-directed chains form a 3D network (ESI:† Table S3).

Crystal and extended structure of 4. Compound 4 crystallizes in the monoclinic P21/c space group. It consists of a Cd(II) monomeric structure, presenting a [CdO4N2] core composed of two asymmetric μ1-η2-ACA ligands and one 1,10-phen, forming a distorted trigonal prismatic geometry (S = 6.397) (Fig. 4a). The bond lengths and bond angles range between 2.2939(17)–2.3637(14) Å and 56.26(5)–154.07(6)° (ESI:† Table S4), presenting similar values to that of other hexacoordinated Cd(II) compounds based on μ1-η2 coordinated carboxylate moieties and 1,10-phen ligands.50,51

Their intermolecular interactions expand the structure along the bc plane, forming a 2D supramolecular structure (Fig. 4b). These interactions are based on the reciprocal N–H···OCOO synthon combined with a π···π pattern between the ACA and 1,10-phen aromatic rings and between the 1,10- phen aromatic rings themselves. In addition, these interactions generate voids with an accessible volume of 361.05 Å3 (9.3% of the unit cell volume, calculated using a probe radius of 1.2 Å),49 where three EtOH molecules hold the monomeric units together through different H-bonds supported by C–H···O associations (Fig. 4c and d and ESI:† Table S4).

Crystal and extended structure of 5. Compound 5 crystallizes in the triclinic $P\bar{1}$ space group. It consists of a Cd(II) monomeric structure, presenting a [CdO4N3] core composed of two asymmetrically μ1-η2-ACA ligands and one terpy adopting an intermediate geometry between capped octahedral (S = 5.471) and capped trigonal prismatic (S = 5.517) (Fig. 5a). The bond lengths and bond angles oscillate between 2.237(2)–2.670(2) Å and 52.74(7)–160.07(7)°, which are similar to that of other heptacoordinated Cd(II) compounds,

presenting carboxylate and terpyridine-based ligands (ESI:† Table S5).52,53 In addition, the supramolecular scaffold of the compound generates voids with an accessible volume of 120.68 Å3 (5.9% of the unit cell volume, calculated using a probe radius of 1.2 Å),49 where two DMF molecules are placed.

Their intermolecular interactions form a 2D plane along the ab axes (Fig. 5b). This expansion is promoted by the N–H···OCOO synthon supported by π···π associations between the terpy aromatic rings as well as weak C–H···O interactions (Fig. 5b and c). Moreover, the DMF molecules hold together the monomeric units via carbonyl oxygen atoms through C– H···O interactions involving the aromatic protons from ACA and terpy ligands of different monomeric units. These interactions extend the structure along the [11¯1] direction, which in combination with the propagation along the ab plane form a 3D network (Fig. 5d and ESI:† Table S5).

Structural overview

Geometric evaluation. The calculated S parameters and average twist angles (ata) for 1–5 are provided in Table 1.

For the hexacoordinated compounds (1, 2 and 4), the S parameter indicates that the trigonal prismatic (1, 4) and octahedral (2) geometries are a better fit, although the values above six in 1 and 4 show important distortions with respect to the ideal trigonal prismatic geometry.39 In 1, the ACA acting as a ligand bridge (O6) generates most of the distortion from the ideal polyhedron, as indicated by its twist angles. The bond angle between the carbonyl oxygen atom and the pyridine nitrogen atom displays a value of 89.33(5)°, while the two chelate angles are 55.98(4)° and 56.69(5)°, which contribute to the distortion. Besides, in complex 4 the presence of three μ1-η2 coordination modes permit a better accommodation to the ideal geometry. Herein, the μ1-η2 coordination of 1,10-phen, which forms a five-membered ring, is considered an important factor for the generated distortion, given that it presents a considerably higher twist angle compared with that of the two four-membered rings of the two carboxylate moieties from ACA. Differently, the absence of μ1-η2 coordinated ligands in 2 avoid important distortions with respect to the ideal octahedral geometry, presenting ata and S values close to that of the ideal geometry (Table 1 and Fig. 6).54 For 3, the S parameter indicates that the capped trigonal prismatic is the most adequate geometry. Herein, the capped position is occupied by the oxygen atom of the carboxylate group with the μ2-η2:η1 coordination mode not involved in the bridge (O1), while the two

faces of the trigonal prism show distortion with respect to the ideal polyhedron, presenting an ata value of 23.64°. Meanwhile, compound 5 does not fit well with a specific geometry, displaying an intermediate form between a capped octahedron and a capped trigonal prism with S values differing by less than 0.1 between these two geometries (Table 1 and Fig. 6).55,56

Structural comparison. The bond angles of 1–5 were analyzed to study the effect generated by the ligands around their Cd(II) cores. The chelate angles of ACA and the bite angles of dPy are summarized in the ESI† (Table S6). The outer atom angles of dPy were also utilized for the analysis given that differently from the bite angles, they consider the planarity of the ligands and their steric effect in the coordination sphere of the complexes.57

The lowest value of the outer atom angle of py in compound 1 (77.04°) permits the introduction of the carbonyl oxygen atom of ACA into the coordination sphere, promoting the formation of the CP. This behavior agrees with other Zn(II) CPs containing ACA and py or 4-phpy, observing a limit outer atom angle of 80.86°.30,31 In 2, the increase in the outer atom angle up to 83.70° does not allow the coordination of the carbonyl oxygen atom of ACA. Instead, two water molecules are coordinated to the Cd(II) center, providing additional stabilization to the structure arising from the strong intramolecular interactions of the coordinated water molecules.58 The introduction of these solvent molecules in the Cd(II) center agrees with the outer atom angle of previous Zn(II) complexes bearing ACA and 4-phenylpyridine (79.42°), allowing the coordination of additional atoms into the coordination sphere (ESI:† Table S6).29

For 3 and 4, the introduction of 2,2′ -bipy and 1,10-phen results in an increase in the outer atom angle in comparison with that of 1 and 2 (ESI:† Table S6). The different nuclearity between 3 and 4 is promoted by the single bond between the aromatic rings of the 2,2′ -bipy, which permit their rotation and better accommodation in the crowded cores. Indeed, the formation of a dimeric structure in 3 is probably influenced by the intra- and intermolecular N–H···OCOO interactions, which force the acetamide moieties to point inside the dimer, differently from previous compounds described in the literature.30,31 In addition, this change in position also influences its supramolecular scaffold given that the non- usual position of the acetamide moieties approach the methyl groups of ACA to the 2,2'-bipy ligands, avoiding the possibility to form interactions involving the aromatic rings such in 1, 2, 4 and 5 (Fig. 7). These results differ from that obtained for Zn(II) complexes

with ACA and 2,2′ -bipy or 1,10-phen ligands, whose bigger outer atom angles yield monomeric arrays. Finally, the coordination of terpy in 5, being a bulkier ligand and presenting an outer atom angle of 217.36°, only allows the formation of the monomeric specie as in its Zn(II) analogue.31

Photophysical properties

UV-vis spectroscopy. All the samples were dissolved in MeOH and their UV-vis spectra recorded at 298 K. Additive measurements were performed for all the compounds and ligands in the concentration range of ∼1 × 10−9 to 1 × 10−4 M to select the optimal concentration at which aggregation does not occur, thus avoiding aggregation caused quenching (ACQ) processes (ESI:† Fig. S21–S23).59 Then, the standards L-tyrosine (L-tyr) for 1–4 and quinine sulphate (QS) for 5 were selected considering that the absorption and emission of 1–5 must fall within the range of the absorption of the selected fluorescence standards with similar intensities.60 The UV-vis spectra of L-tyr and QS were also recorded to obtain the absorptivity values of the standards in the same apparatus for comparison with the complexes to further calculate the corresponding Φ values (ESI:† Fig. S24). Additional details about the absorption maximum (λmax) and molar absorptivity values (ε) of the complexes, ligands and standards are provided in the Experimental section and ESI† (Table S7).

Complexes 1–5 start to aggregate at 3.51 × 10−6 M (1), 3.00 × 10−6 M (2), 1.43 × 10−6 M (3), 5.71 × 10−7 M (4) and 1.99 × 10−7 M (5), presenting bathochromic shifts due to their intermolecular interactions. The aggregation of the complexes leads to the appearance of new bands in their spectra (ESI:† Fig. S23). The formation of patterns of head-to- tail planar interactions such that identified in the structural descriptions of 4 and 5 agree with their aggregation at lower concentrations. Besides, the absence of strong patterns of π···π interactions in 1–3 suggest that they present a lower tendency to form aggregates. Therefore, the UV-vis measurements of 1–5 were performed using 1.00 × 10−7 M solutions, in which aggregation was not observed (ESI:† Fig. S25).

The UV-vis spectra of complexes 1–5 show that their absorption intensity increases in the order of 1 < 5 < 2 < 4 < 3. In these spectra, two bands appear for all the complexes, one at 200–205 nm and the other at 256–281 nm. Moreover, compound 2 shows an additional band in the range of 256– 281 nm, while 5 displays a third band at 330 nm (ESI:† Table S7).

The bands appearing at higher wavelength values are attributed to the metal-to-ligand (MLCT) or ligand-to-metal (LMCT) charge transfer transitions, while that lying at lower energies are associated with the ligand centered (LC) or ligand-to-ligand charge transfer (LLCT) transitions,21 involving either ACA and/or the corresponding dPy ligands.

Photoluminescence. All measurements were performed at 298 K using MeOH solutions of suitable concentrations, as extracted from the UV-vis data, and each complex was irradiated at their maximum excitation wavelength. The emission spectra of 1–5 show that their emission intensity increases in the order of 2 < 1 < 4 < 5 < 3 (Fig. 8). The spectra of 1–4 present one shoulder at ~310 nm, while the emission maxima of all the compounds are centered at 344 (1), 337 (2), 345 (3), 346 (4) and 355 (5) nm. The resultant emission color (λmax-em) for 1–5 at the selected excitation maximum (λexc) is blue violet (1 and 2), bright indigo (3 and 4) and azure (5), according with the CIE 1931 chromaticity diagrams (ESI:† Fig. S26).61 The effect of the coordination of the ligands in the Cd(II) centers was studied by comparing the emission of the free ligands and the resulting compounds excited at the λexc of each complex (ESI:† Fig. S27–S31). Herein, considering that d10 metal complexes present a closed shell configuration, only the charge transfer transitions (CTs) between either the metal and the ligand (MLCT/LMCT) or by the ligand itself (LLCT) are allowed.62,63 The CTs between the π···π* orbitals are less energetic, and thus display bathochromic shifts. In 1–4, the coordination of the ligands results in an important enhancement in their emission intensity with respect to both free ligands. Moreover, these emissions seem to arise from a combination of emissions of both the ACA and dPy ligands owing to the similarity of the curve profiles of these two ligands, which match the emission spectrum of their corresponding complexes. Meanwhile, the emission intensity of 5 is only derived from the terpy ligand given that HACA does not emit when it is excited at 320 nm (ESI:† Fig. S31).

The efficiency of the fluorescence emission of all the complexes was calculated using the fluorescence quantum yield (Φ).64 The relative quantum yield is calculated by determining the Φ of the desired compound and comparing it with that of a fluorescence reference.65

The quantum yields of 1–5 were calculated using eqn (1), as follows:

$$\Phi_s = \Phi_r \left(\frac{OD_r}{OD_s}\right)\left(\frac{I_s}{I_r}\right)\left(\frac{n_s}{n_r}\right)^2 \quad (1)$$

where Φr and Φs are the quantum yields of the reference and sample, respectively. I is the area of the emission spectra, OD is the optical density (or absorbance), and n is the refractive index of the solvent. Herein, L-tyrosine (L-tyr, Φs = 0.14) was used as the standard for 1–4,66 while quinine sulphate (QS, Φs = 0.577) was used for 5,67 given that their emission range falls in the same region. The values of ODr and Ir were obtained using a 1.00 × 10−7 M solution of MilliQ water for L-tyr (nr = 1.3325)68 and a 1.00 × 10−7 M solution of 0.1 M H2SO4 for QS (nr = 1.3325)68 at RT. The values of As and Is of the ligands and 1–5 were recorded at 298 K using 1.00 × 10−7 M solutions with MeOH (ns = 13 314) (ESI:† Fig. S27–S31, respectively).69 The relevant parameters extracted from the photophysical properties of the ligands are provided in the ESI† (Table S7).

The relative quantum yields obtained for 1–5 are 0.99 (1), 0.057 (2), 0.13 (3), 0.069 (4) and 0.65 (5) (Table 2). These Φs values show how the coordination of the ligands to the Cd(II) centers improves their efficiency in all the compounds, avoiding the PET mechanisms of dPy through their coordination. Furthermore, the coordination of the dPy ligands allows the formation of five-membered rings in 3–5, resulting in CHEF, which enhances their fluorescence intensities.18 Compound 1 presents the highest Φs but it should be noted that the uncertainty for this value is probably larger than that of the other compounds owing to its low absorbance intensity, which present a large difference compared with that of the L-tyr standard.60 Given that the terpy ligand of 5 displays two five-membered rings when coordinated to the Cd(II) center, its CHEF effect is more effective, showing a five-fold (3), nine-fold (4) and eleven-fold (2) fluorescent enhancement with respect to the remaining compounds (Table 2). Complex 3 shows CHEF produced by its two 2,2'-bipy ligands, which displays a two-fold enhancement with respect to that of 2 and 4. This difference can be attributed to the presence of CHEF in 3, which is not possible in 2. Besides the difference in Φs between 3 and 4, both presenting CHEF, is attributed to the known nπ* excited states of 1,10-phen, promoting nonradiative decay processes and avoiding low emission Φ values.70 Finally, compound 2 shows the lowest Φs, probably because of the presence of two coordinated water molecules, generating unwanted quenching of its fluorescence (Table 2).71 The comparison of these results with that from our previous work based on Zn(II) complexes31 shows that the higher ionic radius of Cd(II) (0.95 Å) than that of Zn(II) (0.74 Å)23 can avoid the negative effects generated by steric crowding around the metal centers and maximize the positive effects of CHEF, obtaining complexes with enhanced fluorescent efficiencies.

Conclusions

We synthesized and characterized five Cd(II) compounds bearing HACA and a set of N-, N^N- and N^N^N-pyridine ligands with increasing denticity and steric effect around their metal cores. It was shown how the size of the pyridines plays an important role in the final structure of the obtained complexes, allowing the introduction of additional atoms in the coordination sphere, which generates compounds with diverse nuclearity going from a CP (1), to dimeric (3) and monomeric (2, 4, and 5) complexes. The elucidation of the crystal structures of 1–5 permitted the study of their molecular and supramolecular interactions, observing the formation of three hexacoordinated (1, 2, and 4) and two heptacoordinated (3 and 5) complexes, presenting trigonal prismatic (1 and 4), octahedral (2), capped trigonal prismatic (3), and an intermediate form between capped trigonal prismatic and capped octahedral (5) geometries. Furthermore, the carboxylate moieties of ACA display the μ1-η2 coordination modes of the ACA ligands for all the compounds except 2, which displays the μ1-η1 coordination modes of ACA stabilized by strong intramolecular H-bonds between the ACA ligands and the coordinated water molecules. Additionally, compound 3 presents the μ2-η2:η1 coordination mode of ACA, forming a dimeric array. Noteworthily, the coordination of the carbonyl oxygen atom of ACA in 1 was observed, which is responsible for its polymeric structure. The supramolecular structures of all the compounds were studied, observing that the complexes are associated by the N–H···OCOO and N–H···OC O synthons and supported by π···π interactions and weak C–H···O associations, generating 2D (1 and 4) and 3D (2, 3, and 5) supramolecular networks. The photoluminescence properties of 1–5 were measured and their Φs values calculated, observing an enhancement in the Φs of the complexes with respect to the ligands in all cases. Although showing the highest Φs, the value of 1 exhibited high uncertainty owing to its low absorbance compared with that of the L-tyr standard, which made it difficult to compare it with the other complexes. In compound 2, the presence of coordinated water molecules resulted in unwanted quenching of its fluorescence. In contrast, the favorable contributions the CHEF of dPy in 3–5 led to higher Φs values, presenting a good strategy to obtain complexes with enhanced photoluminescence properties.

Experimental section

Materials and general methods

Cadmium(II) acetate dihydrate (Cd(OAc)2·2H2O), α-acetamidocinnamic acid (HACA), pyridine (py), 3-phenylpyridine (3-phpy), 2,2'-bipyridine (2,2'-bipy), 1,10-phenantroline monohydrate (1,10-phen • H2O), and 2,2':6',2''-terpyridine (terpy) ligands; L-tyrosine (L-tyr) and quinine for the preparation of the fluorescence standards; and ethanol (EtOH), methanol (MeOH), dimethylformamide (DMF), diethyl ether (Et2O), sulfuric acid (H2SO4) and MilliQ water solvents were purchased from Sigma-Aldrich. Deuterated dimethylsulfoxide (DMSO-d6) and methanol (MeOH-d4) were purchased from Eurisotop. All reagents were used as received without further purification. All the reactions and manipulations were carried out in air at room temperature (RT). Elemental analyses (C, H, N) were carried on a Thermo Scientific Flash 2000 CHNS analyzer. FTIR-ATR spectra were recorded on a Perkin Elmer spectrometer, equipped with an attenuated total reflectance (ATR) accessory model MKII Golden Gate with a diamond window in the range of 4000–500 cm−1. 1H, 13C{1H} and DEPT-135 NMR spectra were recorded on a Bruker Ascend 400 MHz spectrometer in DMSO-d6 solution for 1–5 and MeOH-d4 for 1 and 2 at RT. All chemical shifts (δ) are presented in ppm relative to TMS as the internal standard. L-Tyrosine (L-tyr) was used as the fluorescence standard for the calculation of the quantum yield (Φ) values of 1–4. For 5, the calculation of Φ was performed using quinine sulphate (QS) as the standard, given that the wavelength corresponding to its maximum effective absorption is outside the range of L-tyr. The electronic spectra in MeOH solutions for all the ligands and 1–5, MilliQ water for L-tyrosine (L-tyr) and 0.1 M H2SO4 solution for quinine were recorded on an Agilent HP 8453 UV-vis spectrophotometer with a quartz cell having a path length of 1 cm in the range of 190–600 nm. The molar absorptivity values were calculated as log(ε). Fluorescence measurements were carried out at 25 °C with a Perkin Elmer LS 55 50 Hz fluorescence spectrometer using a 1 cm quartz cell. The samples were excited at their excitation maximum (λexc) and their emission was recorded between λexc and 2λexc. Both CIE 1931 chromaticity diagrams and corrected dilution effects were performed using the Origin 2019b software.

Synthesis and characterization of complexes 1–5

A Cd(OAc)2·2H2O (100 mg, 0.375 mmol) solution in EtOH (10 mL for 1 and 3–5; 2 mL for 2) was prepared. Then, a mixture of HACA (154 mg, 0.750 mmol) and dPy (0.750

mmol, 1; 1.13 mmol, 2; and 0.375 mmol, 3–5) was dissolved in EtOH (5 mL for 1, 3–5; and 1 mL for 2). The metal solution was added dropwise to the ligand solution at RT and stirred overnight until a white solid precipitated. Afterwards, the reaction crude was kept in a freezer for one day. The resulting white solid was filtered, washed with 10 mL of cold Et2O (repeated twice) and dried under vacuum. Additionally, in the synthesis of 1 and 4, direct precipitation did not occur, and the obtained solutions were concentrated under vacuum to near dryness and kept in a fridge for two days until a white crystalline solid precipitated (1) or forced to precipitation using 10 mL of cold Et2O (4).

The synthesis of suitable crystals for X-ray diffraction was performed using different methods. For 1, its mother liquor was kept in a fridge at 4 °C for seven days. For 2–5, the solid was recrystallized in EtOH and let to evaporate for three days (2) or recrystallized in EtOH for two days (4), MeOH for fifteen days (3), and DMF for six days (5) and kept sealed at RT.

1. Yield: 140 mg (62% based on Cd). Elemental analysis calc. (%) for C27H25CdN3O6 (599.91): C 54.06; H 4.20; N 7.00; found: C 53.98; H 4.01; N 6.84. FTIR-ATR (wavenumber, cm−1): 3209(m) [ν(N–H)], 3165–3003(br) [ν(C–H)ar + ν(C–H)alk], 2946(w) [ν (C − H)al], 1658(w), 1644(w), 1624(m) [ν (C O)], 1604(w), 1574(w), 1552(sh), 1530(s) [vas(COO)], 1521(s), 1489(s) [ν (C C/C N)], 1446(m), 1397(s) [ν s(COO)], 1355(s) [δ (C C/C N)], 1315(m), 1285(m), 1241(w), 1220(w), 1209(m), 1188(w), 1138(w), 1070(w), 1040(m) [δip(C–H)], 1015(w), 988(m) [δip(C–H)], 935(w), 895(w), 846(w), 785(m), 774(s) [δoop(C–H)], 754(m), 704(s) [δoop(C–H)], 689(s) [δoop(C–H)], 651(m), 633(m), 614(m), 565(m), 551(m), 531(m), 523(m). 1H NMR (400 MHz; DMSO-d6; Me4 Si; 298 K): δ = 9.18 [2H, s, NHACA], 8.59 [2H, d, 3J = 4.1 Hz, o-Hpy], 7.81 [1H, td, 3J = 7.6, 4J = 1.6 Hz, p-Hpy], 7.51 [4H, d, 3J = 6.7 Hz, o-HACA], 7.41 [2H, m, m-Hpy], 7.35 [4H, t, 3J = 7.2 Hz, m-HACA], 7.29 [4H, s, p-HACA + HN–C–CHACA], 1.96 [6H, s, CO–CH3,ACA]. 1H NMR (400 MHz; MeOH-d4; Me4Si; 298 K): δ = 8.61 [2H, d, 3J = 6.0 Hz, 4J = 1.6 Hz, o-Hpy], 7.87 [1H, tt, 3J = 7.8, 4J = 1.7 Hz, p-Hpy], 7.47 [6H, m, o-HACA + m-HACA], 7.37 [1H, s, HN–C–CHACA], 7.27 [6H, m, p-HACA + m-Hpy], 2.04 [6H, s, CO–CH3,ACA].13C{1H} NMR (400 MHz; DMSO-d6; Me4Si; 298 K): δ = 171.54 [HN–COACA], 168.51 [COOACA], 149.76 [o-Cpy], 137.26 [p-Cpy], 135.26 [O2C–CACA], 129.68 [HN–C–CH–CACA], 129.42 [o-CACA], 129.18 [p-CACA], 128.43 [m-CACA], 128.25 [HN–C–CHACA], 124.39 [m-Cpy], 23.16 [OC–CH3,ACA]. 13C{1H} NMR (400 MHz; MeOH-d4; Me4Si; 298 K): δ = 174.05 [HN–COACA], 172.95

[COOACA], 150.59 [o-Cpy], 139.40 [p-Cpy], 135.99 [O2CCACA], 132.52 [HN–C–CHACA], 130.52 [o-CACA], 130.03 [HN–C–CH–CACA], 129.75 [p-CACA], 129.52 [m-CACA], 125.91 [m-Cpy], 22.85 [OC–CH3,ACA]. DEPT-135 NMR (400 MHz; DMSO-d6; Me4Si; 298 K): δ = 149.75 [o-Cpy], 137.22 [p-Cpy], 129.41 [o-CACA], 129.17 [p-CACA], 128.43 [m-CACA], 128.25 [HN–C–CHACA], 124.38 [m-Cpy], 23.16 [OC–CH3,ACA]. DEPT-135 NMR (400 MHz; MeOH-d4; Me4Si; 298 K): δ = 150.59 [o-Cpy], 139.41 [p-Cpy], 132.52 [HN–C–CHACA], 130.52 [o-CACA], 129.75 [p-CACA], 129.52 [m-CACA], 125.91 [m-Cpy], 22.85 [OC–CH3,ACA]. UV-vis (MeOH, 1.00 × 10−9–1.37 × 10−4 M): λmax (log ε) = 200 nm (4.75), 276 nm (4.62). Fluorescence (MeOH, 1.00 × 10−7 M): λexc = 229 nm; λmax-em (Φ based on L-tyr) = 344 nm (0.99).

2. Yield: 203 mg (60% based on Cd). Elemental analysis calc. (%) for C44H46CdN4O10 (903.25): C 58.51; H 5.13; N 6.20; found: C 58.28; H 5.01; N 5.94. FTIR-ATR (wavenumber, cm−1): 3638(m) [ν(O–H)], 3299(m) [ν(O–H)], 3203(m) [ν(N–H)], 3147–3024(br) [ν(C–H)ar + ν(C–H)alk], 2980–2656(br) [ν(C–H)al], 1670(m) [ν (C O)], 1648(w), 1635(w), 1595(w), 1585(w), 1559(s) [ν as(COO)], 1518(s) [ν (C C/C N)], 1489(m), 1474(m), 1449(m), 1389(s) [ν s(COO)], 1357(s) [δ (C C/C N)], 1315(w), 1282(s), 1209(w), 1199(w), 1157(w), 1140(w), 1112(w), 1077(w), 1029(w) [δip(C–H)], 1012(w) [δip(C–H)], 984(w), 957(w), 932(w), 920(w), 897(w), 848(w), 821(w), 764(s) [δoop(C–H)], 743(s) [δoop(C–H)], 710(s), 692(s) [δoop(C–H)], 646(s), 626(s), 589(w), 563(s), 557(s), 526(s). 1H NMR (400 MHz; DMSO-d6; Me4 Si; 298 K): δ = 9.17 [2H, s, NHACA], 8.88 [2H, d, 4J = 2.0 Hz, o-Hpy], 8.57 [2H, dd, 3J = 4.8 Hz, 4J = 1.5 Hz, o-Hpy], 8.08 [2H, ddd, 3J = 8.0 Hz, 4J = 2.4 Hz, 1.6 Hz, p-Hpy], 7.72 [4H, m, o-Hph(3-phpy)], 7.50 [10H, m, o-HACA + m-Hpy + m-Hph(3-phpy)], 7.43 [2H, m, p-Hph(3-phpy)], 7.35 [4H, t, 3J = 7.5 Hz, m-HACA], 7.28 [2H, d, 3J = 7.4 Hz, p-HACA], 7.26 [2H, s, HN–C–CHACA], 1.96 [6H, s, OC–CH3,ACA]. 1H NMR (400 MHz; MeOH-d4; Me4 Si; 298 K): δ = 8.81 [2H, s, o-Hpy], 8.52 [2H, d, 3J = 4.3 Hz, o-Hpy], 8.08 [2H, ddd, 3J = 8.0 Hz, 4J = 2.3 Hz, 1.6 Hz, p-Hpy], 7.62 [4H, ddd, 3J = 4.5 Hz, 4J = 3.6 Hz, 1.9 Hz, o-Hph(3-phpy)], 7.51 [2H, dd, 3J = 8.0 Hz, 4J = 5.0 Hz, p-Hph(3-phpy)], 7.36 [16H, m, o-HACA + m-HACA + p-HACA, HN-C-CHACA, m-Hpy + m-Hph(3-phpy)], 2.04 [6H, s, OC–CH3,ACA]. 13C{1H} NMR (400 MHz; DMSO-d6; Me4Si; 298 K): δ = 171.39 [HN–COACA], 168.44 [COOACA], 148.59 [o-Cpy], 147.71 [o-Cpy], 137.13 [py-Cph(3-phpy)], 135.76 [m-Cpy], 135.23 [O2C–CACA], 134.42 [p-Cpy], 129.65 [HN–C–CH-CACA], 129.38 [o-CACA], 129.31 [m-Cph(3-phpy)], 129.05 [p-CACA], 128.40 [p-Cph(3-phpy)], 128.33 [m-CACA],

128.21 [HN–C–CHACA], 127.02 [o-Cph(3-phpy)], 124.11 [m-CHpy], 23.11 [OC–CH3,ACA]. 13C{1H} NMR (400 MHz; DMSO-d6; Me4 Si; 298 K): δ = 173.91 [HN–COACA], 172.87 [COOACA], 149.04 [o-Cpy], 148.66 [o-Cpy], 138.92 [py-Cph(3-phpy)], 138.30 [m-Cpy], 137.14 [p-Cpy], 135.98 [O2C–CACA], 132.45 [o-CACA], 130.52 [m-CACA], 130.30 [p-CACA], 130.07 [HN–C–CH–CACA], 129.74 [HN–C–CHACA], 129.56 [p-Cph(3-phpy)], 129.51 [o-Cph(3-phpy)], 128.16 [m-Cph(3-phpy)], 125.75 [m-CHpy], 22.85 [OC–CH3,ACA]. DEPT-135 NMR (400 MHz; DMSO-d6; Me4Si; 298 K): δ = 148.59 [o-Cpy], 147.71 [o-Cpy], 134.42 [p-Cpy], 129.38 [o-CACA], 129.31 [m-Cph(3-phpy)], 129.05 [p-CACA], 128.40 [p-Cph(3-phpy)], 128.33 [m-CACA], 128.21 [HN–C–CHACA], 127.01 [o-Cph(3-phpy)], 124.12 [m-CHpy], 23.12 [OC-CH3,ACA]. DEPT-135 NMR (400 MHz; MeOH-d4; Me4Si; 298 K): δ = 149.04 [o-Cpy], 148.65 [o-Cpy], 137.14 [p-Cpy], 132.45 [o-CACA], 130.52 [m-CACA], 130.29 [p-CACA], 129.74 [HN–C–CHACA], 129.56 [p-Cph(3-phpy)], 129.50 [o-Cph(3-phpy)], 128.15 [m-Cph(3-phpy)], 125.75 [m-CHpy], 22.84 [OC–CH3,ACA]. UV-vis (MeOH, 2.43 × 10−9–6.55 × 10−5 M): λmax (log ε) = 204 nm (4.78), 256 nm (4.56), 274 nm (4.53). Fluorescence (MeOH, 1.00 × 10−7 M): λexc = 229 nm; λmax-em (Φ based on L-tyr) = 337 nm (0.057).

3. Yield: 205 mg (77% based on Cd). Elemental analysis calc. (%) for C66H64Cd2N8O14 (1418.08): C 55.90; H 4.55; N 7.90; found: C 55.78; H 4.43; N 7.74. FTIR-ATR (wavenumber, cm−1): 3388(br) [ν(O–H)], 3248(m) [ν(N–H)], 3198–3004(br) [ν(C–H)ar + ν(C–H)alk], 2924 (w) [ν(C–H)al], 1693(w), 1670(w) [ν (C O)], 1648(w), 1597(w), 1533(s) [ν as(COO)], 1514(s) [ν as(COO)], 1491(m), 1478(w), 1440(m) [ν (C C/C N)], 1389(s) [ν s(COO)], 1369(s), 1355(s) [δ (C C/C N)], 1319(m), 1288(m), 1252(m), 1211(w), 1183(w), 1175(w), 1159(w), 1122(w), 1077(w), 1059(w), 1019(s) [δip(C–H)], 965(w), 958(w), 923(w), 891(w), 849(w), 819(w), 785(w), 778(s) [δoop(C–H)], 767(s) [δoop(C–H)], 752(m), 739(m), 718(w), 687(s) [δoop(C–H)], 649(m), 604(m), 592(s), 543(s), 525(s). 1H NMR (400 MHz; DMSO-d6; Me4Si; 298 K): 9.16 [2H, s, NHACA], 8.81 [2H, d, 3J = 3.7 Hz, o-Hpy], 8.52 [2H, d, 3J = 7.9 Hz, m-Hpy], 8.13 [2H, t, 3J = 7.5 Hz, p-Hpy], 7.65 [2H, m, m-Hpy], 7.47 [4H, d, 3J = 5.8 Hz, o-HACA], 7.33 [4H, m, m-HACA], 7.26 [4H, m, p-HACA + HN–C–CHACA], 1.95 [6H, s, OC–CH3,ACA]. 13C{1H} NMR (400 MHz; DMSO-d6; Me4 Si; 298 K): δ = 171.12 [HN–COACA], 168.38 [COOACA], 150.56 [o-Cpy], 149.88 [o-CHpy], 139.71 [p-Cpy], 135.35 [O2C–CACA], 129.90 [HN–C–CH–CACA], 129.34 [o-CACA], 128.65 [p-CACA], 128.36 [m-HACA], 128.10 [HN–C–CHACA], 125.81 [m-Cpy], 121.95 [m-Cpy], 23.17 [OC-CH3,ACA]. DEPT-135 NMR (400

MHz; DMSO-d6; Me4Si; 298 K): δ = 149.87 [o-CHpy], 139.71 [p-Cpy], 129.34 [o-CACA], 128.66 [p-CACA], 128.35 [m-HACA], 128.10 [HN–C–CHACA], 125.81 [m-Cpy], 121.95 [m-Cpy], 23.17 [OC-CH3,ACA]. UV-vis (MeOH, 5.50 × 10−10–2.94 × 10−5 M): λmax (log ε) = 203 nm (5.34), 279 nm (5.12). Fluorescence (MeOH, 1.00 × 10−7 M): λexc = 229 nm; λmax-em (Φ based on L-tyr) = 345 nm (0.13).

4. Yield: 208 mg (66% based on Cd). Elemental analysis calc. (%) for C40H46CdN4O9 (839.22) C 57.25; H 5.52; N 6.68; found: C 57.04; H 5.28; N 6.43. FTIR-ATR (wavenumber, cm−1): 3365(w) [ν(O–H)], 3216(w) [ν(N–H)], 3180–3021(br) [ν(C–H)ar + ν(C–H)alk], 2999–2884(br) [ν(C–H)al], 1682(m), 1667(m) [ν (C O)], 1640(w), 1554(m), 1540(br), 1519(s) [ν as(COO)], 1488(s) [ν (C C/C N)], 1448(m), 1428(sh), 1396(s) [ν s(COO)], 1360(s) [δ (C C/C N)], 1268(m), 1207(w), 1142(w), 1101(w), 1081(w), 1042(w) [δip(C–H)], 1002(w), 980(w), 929(w), 894(w), 866(w), 845(m), 775(sh), 766(s) [δoop(C–H)], 754(sh), 725(s) [δoop(C–H)], 693(s) [δoop(C–H)], 656(w), 642(m), 621(m), 593(m), 556(m), 524(s). 1H NMR (400 MHz; DMSO-d6; Me4Si; 298 K): δ = 9.19 [2H, d, 3J = 3.2 Hz, o-Hpy], 9.12 [2H, s, NHACA], 8.80 [2H, d, 3J = 8.1 Hz, p-Hpy], 8.21 [2H, s, Hph(1,10-phen)], 8.05 [2H, dd, 3J = 7.9 Hz, 4J = 4.7 Hz, m-Hpy], 7.45 [4H, d, 3J = 6.4 Hz, o-HACA], 7.32 [4H, t, 3J = 7.2 Hz, m-HACA], 7.25 [2H, d, 3J = 7.2 Hz, p-HACA], 7.22 [2H, s, HN–C–CHACA], 1.93 [6H, s, OC–CH3,ACA]. 13C{1H} NMR (400 MHz; DMSO-d6; Me4Si; 298 K): δ = 170.52 [HN–COACA], 168.14 [COOACA], 150.31 [o-CHpy], 140.28 [o-Cpy], 139.05 [p-CHpy], 135.24 [O2C–CACA], 129.82 [HN–C–CH–CACA], 129.24 [o-CACA], 128.64 [m-Cpy], 128.35 [p-CACA], 128.21 [m-CACA], 127.94 [HN–C–CHACA], 126.97 [CHph(1,10-phen)], 125.10 [m-CHpy], 23.05 [OC–CH3,ACA]. DEPT-135 NMR (400 MHz; DMSO-d6; Me4Si; 298 K): δ = 150.31 [o-CHpy], 139.05 [p-CHpy], 129.24 [o-CACA], 128.37 [p-CACA], 128.22 [m-CACA], 127.94 [HN–C–CHACA], 126.98 [CHph(1,10-phen)], 125.10 [m-CHpy], 23.06 [OC–CH3,ACA]. UV-vis (MeOH, 1.00 × 10−9–7.06 × 10−5 M): λmax (log ε) = 205 nm (4.97), 269 nm (4.96). Fluorescence (MeOH, 1.00 × 10−7 M): λexc = 229 nm; λmax-em (Φ based on L-tyr) = 346 nm (0.069).

5. Yield: 220 mg (65% based on Cd). Elemental analysis calc. (%) for C43H45CdN7O8 (900.27) C 57.37; H 5.04; N 10.89; found: C 57.12; H 4.93; N 10.77. FTIR-ATR (wavenumber, cm−1): 3329(w), 3210(w) [ν(N–H)], 3084–3024(br) [ν(C–H)ar + ν (C – H)alk], 2999 – 2945(br) [ν (C – H)al], 1703(w) [ν (C═O)DMF], 1675(m) [ν

(C═O)ACA], 1642(w), 1575(m), 1547(s), 1536(sh) [ν as(COO)], 1488(m), 1476(m) [ν (C═C/C═N)], 1447(m), 1441(sh), 1406(sh) [ν s(COO)], 1381(s) [δ (C═C/C═N)], 1373(sh), 1359(sh), 1315(m), 1255(m), 1207(w), 1190(w), 1163(w), 1101(w), 1076(w), 1036(w), 1013(m) [δip(C–H)], 976(w), 921(w), 891(w), 843(w), 831(w), 796(w), 771(s) [δoop(C–H)], 749(m), 731(m), 689(s) [δoop(C–H)], 651(m), 637(m), 624(m), 604(m). 1H NMR (400 MHz; DMSO-d6; Me4Si; 340 K): δ = 8.99 [2H, d, 3J = 4.3 Hz, o-Hpy], 8.79 [2H, s, NHACA], 8.64 [4H, m, m-Hpy-side + m-Hpy-center], 8.36 [1H, t, 3J = 8.0 Hz, p-Hpy-center], 8.20 [2H, td, 3J = 7.8 Hz, 4J = 1.6 Hz, p-Hpy-side], 7.74 [2H, dd, 3J = 7.0 Hz, 3J = 5.2 Hz, m-Hpy-side], 7.45 [4H, m, o-HACA], 7.32 [4H, m, m-HACA], 7.23 [4H, m, p-HACA + HN–C–CHACA], 1.90 [6H, s, OC–CH3,ACA]. 13C NMR (400 MHz; DMSOd6; Me4Si; 298 K): δ = 170.99 [HN–COACA], 167.96 [COOACA], 150.35 [o-CHpy-side], 149.31 [o-Cpy-center], 148.47 [o-CHpy-side], 142.04 [p-Cpy-center], 140.24 [p-Cpy-side], 135.51 [O2C–CACA], 129.71 [HN–C–CH–CACA], 129.22 [o-CACA], 128.22 [p-CACA + m-CACA], 127.87 [HN–C–CHACA], 126.53 [m-Cpy-side], 123.17 [m-Cpy-side], 122.66 [m-Cpy-center], 23.22 [OC–CH3,ACA]. DEPT-135 NMR (400 MHz; DMSO-d6; Me4 Si; 298 K): δ = 150.33 [o-CHpy-side], 142.00 [p-Cpy-center], 140.30 [p-Cpy-side], 129.20 [o-CACA], 128.22 [p-CACA], 127.88 [m-CACA + HN–C–CHACA], 126.54 [m-Cpy-side], 123.12 [m-Cpy-side], 122.64 [m-Cpy-center], 23.19 [OC–CH3,ACA]. UV-vis (MeOH, 1.00 × 10−9–6.31·10−5 M): λmax (log ε) = 203 nm (5.27), 281 nm (4.95), 320 nm (4.43). Fluorescence (MeOH, 1.00 × 10−7 M): λexc = 320 nm; λmax-em (Φ based on QS) = 355 nm (0.65).

X-ray crystallographic data

For compounds 1–5, colorless prism-like specimens were used for the X-ray crystallographic analysis. The X-ray intensity data were measured on a D8 Venture system equipped with a multilayer monochromate and Mo microfocus (λ = 0.71073 Å). The frames were integrated with the Bruker SAINT Software package using a narrow-frame algorithm. All hydrogen atoms were refined using a riding model (AFIX) with an isotropic temperature factor equal to 1.2, and thus the bond lengths of X–H were fixed. For 1, the integration of the data yielded 7615 independent reflections (Rsig = 2.87%) and 6430 (84.44%) were greater than 2σ(|F|2). For 2, the integration of the data yielded 6266 independent reflections (Rsig = 1.88%) and 5565 (88.81%) were greater than 2σ(|F|2). For 3, the integration of the data yielded 10 043 independent reflections (Rsig = 3.35%) and 8961 (89.23%) were greater than 2σ(|F|2). For 4, the integration of the data yielded 11 696 independent reflections (Rsig

= 3.70%) and 9642 (82.44%) were greater than 2σ(|F|2). For 5, the integration of the data yielded 12 616 independent reflections (Rsig = 2.76%) and 10 746 (85.18%) were greater than 2σ(|F|2).

The structures were solved and refined using SHELX (version 2018/3).72 The final cell constants and volume are based on the refinement of the XYZ-centroids of the reflections above 20σ(I). Data were corrected for absorption effects using the multi-scan method (SADABS). The crystal data and relevant details of the structure refinement for compounds 1–5 are reported in Tables 3 and 4.

Complete information about the crystal structure and molecular geometry is available in CIF format via CCDC 2124508 (1), 2124510 (2), 2124511 (3), 2124509 (4), 2124512 (5). Molecular graphics were generated using the Mercury 4.3.1 software73–75 using the POV-ray image package.76 The color codes for all the molecular graphics are light orange (Cd), red (O), light blue (N), dark gray (C), and white (H).

Author Contributions

Conceptualization, J. P.; data curation, D. E. and M. F.-B.; formal analysis, D. E. and M. F.-B.; funding acquisition, J. P.; investigation, D. E.; methodology, D. E.; project administration, J. P.; resources, J. P.; T. C.; software, D. E.; supervision, J. P.; validation, J. P. and T. C.; visualization, D. E.; writing-original draft preparation, D. E.; writing-review and editing, J. P., T. C. All authors have read and agreed to the published version of the manuscript.

Conflicts of Interest

There are no conflicts to declare.

Acknowledgements

J. P. acknowledges financial support from the CB615921 project, the CB616406 project from “Fundació La Caixa”, and the 2017SGR1687 project from the Generalitat de Catalunya. D. E. acknowledges the PIF predoctoral fellowship from the Universitat Autònoma de Barcelona.

References

1 R. Kumar, A. Sharma, H. Singh, P. Suating, H. S. Kim, K. Sunwoo, I. Shim, B. C. Gibb and J. S. Kim, Chem. Rev., 2019, 119, 9657–9721.

2 H. Wang, X. Ji, Z. A. Page and J. L. Sessler, Mater. Chem. Front., 2020, 4, 1024–1039.

3 A. M. Alsharabasy, A. Pandit and P. Farràs, Adv. Mater., 2021, 33, 2003883.

4 R. Adam, M. Mon, R. Greco, L. H. G. Kalinke, A. Vidal-Moya, A. Fernandez, R. E. P. Winpenny, A. Doménech-Carbó, A. Leyva-Pérez, D. Armentano, E. Pardo and J. Ferrando-Soria, J. Am. Chem. Soc., 2019, 141, 10350–10360.

5 X.-G. Yang, X.-M. Lu, Z.-M. Zhai, Y. Zhao, X.-Y. Liu, L.-F. Ma and S.-Q. Zang, Chem. Commun., 2019, 55, 11099–11102.

6 J.-H. Qin, Y.-D. Huang, Y. Zhao, X.-G. Yang, F.-F. Li, C. Wang and L.-F. Ma, Inorg. Chem., 2019, 58, 15013–15016.

7 X.-G. Yang, X.-M. Lu, Z.-M. Zhai, J.-H. Qin, X.-H. Chang, M.-L. Han, F.-F. Li and L.-F. Ma, Inorg. Chem. Front., 2020, 7, 2224–2230.

8 B. J. Holliday and C. A. Mirkin, Angew. Chem., Int. Ed., 2001, 40, 2022–2043.

9 Z. Ji, R. Freund, C. S. Diercks, P. Hirschle, O. M. Yaghi and S. Wuttke, Adv. Mater., 2021, 2103808.

10 Y. He, S. Xiang and B. Chen, J. Am. Chem. Soc., 2011, 133, 14570–14573.

11 J. Su, J. Zhang, X. Tian, M. Zhao, T. Song, J. Yu, Y. Cui, G. Qian, H. Zhong, L. Luo, Y. Zhang, C. Wang, S. Li, J. Yang, H. Zhou, J. Wu and Y. Tian, J. Mater. Chem. B, 2017, 5, 5458–5463.

12 E. Molenbroek, N. Straathof, S. Dück, Z. Rashid, J. H. van Lenthe, M. Lutz, A. Gandubert, R. J. M. Klein Gebbink, L. De Cola and S. Bonnet, Dalton Trans., 2013, 42, 2973–2984.

13 Y. Jeong, Y.-M. Kook, K. Lee and W.-G. Koh, Biosens. Bioelectron., 2018, 111, 102–116.

14 C. V. Esteves, J. Costa, H. Bernard, R. Tripier and R. Delgado, New J. Chem., 2020, 44, 6589–6600.

15 N. Sinha, L. Stegemann, T. T. Y. Tan, N. L. Doltsinis, C. A. Strassert and F. E. Hahn, Angew. Chem., Int. Ed., 2017, 56, 2785–2789.

16 A. Rodriguez-Serrano, V. Rai-Constapel, M. C. Daza, M. Doerr and C. M. Marian, Phys. Chem. Chem. Phys., 2015, 17, 11350–11358.

17 B. C. De Simone, G. Mazzone, N. Russo, E. Sicilia and M. Toscano, Molecules, 2016, 21, 1093.

18 R. D. Hancock, Chem. Soc. Rev., 2013, 42, 1500–1524.

19 N. J. Williams, W. Gan, J. H. Reibenspies and R. D. Hancock, Inorg. Chem., 2009, 48, 1407–1415.

20 Z. Dai, Molecules, 2016, 21, 1647.

21 A. Barbieri, G. Accorsi and N. Armaroli, Chem. Commun., 2008, 2185–2193.

22 S. Purkait, G. Aullón, E. Zangrando and P. Chakraborty, Dalton Trans., 2017, 46, 2184–2195.

23 R. D. Shannon, Acta Crystallogr., Sect. A: Cryst. Phys., Diffr., Theor. Gen. Crystallogr., 1976, 32, 751–767.

24 A. L. Allred, J. Inorg. Nucl. Chem., 1961, 17, 215–221.

25 Y. Mikata, A. Kizu, K. Nozaki, H. Konno, H. Ono, S. Mizutani and S. Sato, Inorg. Chem., 2017, 56, 7404–7415.

26 L. E. Tucker, G. C. Littman, S. Uritis, J. W. Nugent, R. P. Thummel, J. H. Reibenspies, S. B. Jones, H.-S. Lee and R. D. Hancock, Inorg. Chem., 2020, 59, 13117–13127.

27 S. M. Vickers, P. D. Frischmann and M. J. MacLachlan, Inorg. Chem., 2011, 50, 2957–2965.

28 M. Wang, J. Zhang, Y. Sun, J. Wei, C. Tan and X.-F. Wang, CrystEngComm, 2020, 22, 3965–3974.

29 D. Ejarque, F. Sánchez-Férez, T. Calvet, M. Font-Bardia and J. Pons, Inorg. Chim. Acta, 2020, 509, 119695.

30 D. Ejarque, T. Calvet, M. Font-Bardia and J. Pons, Molecules, 2020, 25, 3615.

31 D. Ejarque, T. Calvet, M. Font-Bardia and J. Pons, CrystEngComm, 2021, 23, 6199–6213.

32 G. B. Deacon and R. J. Phillips, Coord. Chem. Rev., 1980, 33, 227–250.

33 T. Hiraoka and S. Shigeto, Phys. Chem. Chem. Phys., 2020, 22, 17798–17806.

34 K. Nakamoto, Infrared and Raman Spectra of Inorganic and Coordination Compounds: Part A: Theory and Applications in Inorganic Chemistry, Wiley Interscience, Hoboken, New Jersey, USA, 6th edn, 2009.

35 I. Fleming and D. Williams, Spectroscopic Methods in Organic Chemistry, Springer International Publishing, Cham, Switzerland, 7th edn, 2019.

761 36 M. X. Zhu, W. Lu, N. Zhu and C. M. Che, Chem. – Eur. J., 2008, 14, 9736–9746.

762 37 F. K.-W. Hau, H.-S. Lo and V. W.-W. Yam, Chem. – Eur. J., 2016, 22, 3738–3749.

763 38 M. Llunell, D. Casanova, J. Cirera, P. Alemany and S. Alvarez, SHAPE v.2.1. Program for
764 the Stereochemical Analysis of Molecular Fragments by Means of Continuous Shape
765 Measures and Associated Tools, Universitat de Barcelona, Barcelona, 2013.

766 39 M. Pinsky and D. Avnir, Inorg. Chem., 1998, 37, 5575–5582.

767 40 P. M. Morse and G. S. Girolami, J. Am. Chem. Soc., 1989, 111, 4114–4116.

768 41 J. C. Friese, A. Krol, C. Puke, K. Kirschbaum and D. M. Giolando, Inorg. Chem., 2000, 39,
769 1496–1500.

770 42 B. Liu, H.-F. Zhou, L. Hou, J.-P. Wang, Y.-Y. Wang and Z. Zhu, Inorg. Chem., 2016, 55,
771 8871–8880.

772 43 M. Sutradhar, T. Roy Barman, E. C. B. A. Alegria, H. M. Lapa, M. F. C. Guedes da Silva and
773 A. J. L. Pombeiro, New J. Chem., 2020, 44, 9163–9171.

774 44 D. Singh and J. B. Baruah, Cryst. Growth Des., 2012, 12, 2109–2121.

775 45 P. Saxena and N. Thirupathi, Polyhedron, 2015, 98, 238–250.

776 46 L.-L. Kong, S. Gao, L.-H. Huo and S. W. Ng, Acta Crystallogr., Sect. E: Struct. Rep. Online,
777 2007, 63, m2938–m2939.

778 47 H. Lin-Xin, L. Lu, W. Jun, X. Bin and Z. Li-Ke, Synth. React. Inorg., Met.-Org., Nano-Met.
779 Chem., 2015, 45, 695–699.

780 48 W. P. Wu, J. Wang, L. Lu, B. Xie, Y. Wu and A. Kumar, Russ. J. Coord. Chem., 2016, 42,
781 71–80.

782 49 A. L. Spek, J. Appl. Crystallogr., 2003, 36, 7–13.

783 50 P. K. Yadav, N. Kumari, P. Pachfule, R. Banerjee and L. Mishra, Cryst. Growth Des., 2012,
784 12, 5311–5319.

785 51 J. Nath, A. Tarai and J. B. Baruah, ACS Omega, 2019, 4, 18444–18455.

786 52 L. Gou, B. Zhang, H.-M. Hu, X.-L. Chen, B.-C. Wang, Q.-R. Wu, T. Qin and Z.-X. Tang, J.
787 Mol. Struct., 2008, 889, 244–250.

788 53 L. Saghatforoush, L. V. Matarranz, F. Chakabian, S. Ghammamy and F. Katouzian, J. Chem.
789 Sci., 2012, 124, 577–585.

790 54 S. Alvarez, Chem. Rev., 2015, 115, 13447–13483.

791 55 D. Casanova, P. Alemany, J. M. Bofill and S. Alvarez, Chem. – Eur. J., 2003, 9, 1281–1295.

792 56 S. Alvarez, P. Alemany, D. Casanova, J. Cirera, M. Llunell and D. Avnir, Coord. Chem. Rev.,
793 2005, 249, 1693–1708.

794 57 F. Sánchez-Férez, J. M. Rius-Bartra, T. Calvet, M. Font-Bardia and J. Pons, Inorg. Chem.,
795 2021, 60, 3851–3870.

796 58 J. M. Andrić, G. V. Janjić, D. B. Ninković and S. D. Zarić, Phys. Chem. Chem. Phys., 2012,
797 14, 10896–10898.

798 59 Y. Hong, J. W. Y. Lam and B. Z. Tang, Chem. Soc. Rev., 2011, 40, 5361–5388.

799 60 M. Levitus, Methods Appl. Fluoresc., 2020, 8, 033001.

800 61 P. J. Alessi, E. C. Carter, M. D. Fairchild, R. W. G. Hunt, C. S. McCamy, B. Kránicz, J. R.
801 Moore, L. Morren, J. H. Noobs, Y. Ohno, M. R. Pointer, D. C. Rich, A. R. Robertson, J. D.
802 Schanda, R. Sève, P. W. Trezona, K. Witt and H. Yaguchi, CIE 15: Technical Report:
803 Colorimetry, International Comimission on Illumination, Washington, D.C., 3rd edn, 2004.

804 62 J. E. Huheey, E. A. Keiter and R. L. Keiter, Inorganic chemistry: principles of structure and
805 reactivity, HarperCollins College Publishers, New York, 4th edn, 1993.

806 63 D. Sutton, Electronic Spectra of Transition Metal Complexes, McGraw-Hill, London, UK,
807 1975.

808 64 M. E. Sommer, M. Elgeti, P. W. Hildebrand, M. Szczepek, K. P. Hofmann and P. Scheerer, in
809 Methods in Enzymology, Elsevier Inc., 1st edn, 2015, vol. 556, pp. 563–608.

810 65 C. Würth, M. Grabolle, J. Pauli, M. Spieles and U. Resch-Genger, Nat. Protoc., 2013, 8, 1535–
811 1550.

812 66 R. F. Chen, Anal. Lett., 1967, 1, 35–42.

813 67 J. W. Eastman, Photochem. Photobiol., 1967, 6, 55–72.

814 68 G. M. Hale and M. R. Querry, Appl. Opt., 1973, 12, 555–563.

815 69 H. El-Kashef, Phys. B, 2000, 279, 295–301.

816 70 G. Accorsi, A. Listorti, K. Yoosaf and N. Armaroli, Chem. Soc. Rev., 2009, 38, 1690–1700.

817 71 F. Doettinger, Y. Yang, M.-A. Schmid, W. Frey, M. Karnahl and S. Tschierlei, Inorg. Chem.,
818 2021, 60, 5391–5401.

72 G. M. Sheldrick, Acta Crystallogr., Sect. A: Found. Crystallogr., 2008, 64, 112–122.

73 C. F. Macrae, P. R. Edgington, P. McCabe, E. Pidcock, G. P. Shields, R. Taylor, M. Towler and J. van de Streek, J. Appl. Crystallogr., 2006, 39, 453–457.

74 C. F. Macrae, I. J. Bruno, J. A. Chisholm, P. R. Edgington, P. McCabe, E. Pidcock, L. Rodriguez-Monge, R. Taylor, J. van de Streek and P. A. Wood, J. Appl. Crystallogr., 2008, 41, 466–470.

75 C. F. MacRae, I. Sovago, S. J. Cottrell, P. T. A. Galek, P. McCabe, E. Pidcock, M. Platings, G. P. Shields, J. S. Stevens, M. Towler and P. A. Wood, J. Appl. Crystallogr., 2020, 53, 226–235.

76 Persistence of Vision Pty. Ltd., Persistence of Vision (TM) Raytracer, Persistence of Vision Pty. Ltd., Williamstown, Australia, 2004.

840 **Table 1**. Geometry distortion analysis of the Cd(II) cores in 1–5 using S parameter calculated
841 with SHAPE,38,39 and ata values40,41

842

Compound	Geometry[a]	S value	ata value (°)	Twist angles[b] (°)
1	OC-6	8.968	21.61	N(3)–Cg(4)–Cg(5)–O(6): 18.87
	TPR-6	**6.631**		O(2)–Cg(4)–Cg(5)–O(1): 18.84
				O(5)–Cg(4)–Cg(5)–O(4): 27.11
2	**OC-6**	**0.054**	59.67	O(4)–Cg(2)–Cg(3)–N(2): 58.79
	TPR-6	16.480		O(1)–Cg(2)–Cg(3)–O(4): 60.81
				N(2)–Cg(2)–Cg(3)–O(1): 59.40
3	PBPY-7	6.197	23.64	N(3)–Cg(2)–Cg(3)–N(4): 23.63
	COC-7	6.472		O(2)#1–Cg(2)–Cg(3)–O(5): 15.81
	CTPR-7	**5.477**		O(2)–Cg(2)–Cg(3)–O(4): 31.48
4	OC-6	10.444	18.83	O(1)–Cg(5)–Cg(6)–O(2): 17.18
	TPR-6	**6.397**		O(4)–Cg(5)–Cg(6)–O(5): 12.98
				N(4)–Cg(5)–Cg(6)–N(3): 26.34
5	PBPY-7	9.349	46.10	N(3)–Cg(4)–Cg(5)–N(4): 46.04
	COC-7	**5.471**		O(4)–Cg(4)–Cg(5)–O(2): 65.95
	CTPR-7	**5.517**		O(5)–Cg(4)–Cg(5)–N(5): 26.32

Close values are highlighted in bold. [a] OC-6 = octahedron; TPR-6 = trigonal prism; PBPY-7 = pentagonal bipyramid; COC-7 = capped octahedron; CTPR-7 = capped trigonal prism. [b] **1**: Cg(4) = O(2) N(3) O(5); Cg(5) = O(1) O(4) O(6). **2**: Cg(2) = O(1) O(4) N(2); Cg(3) = O(1)#1 O(4)#1 N(2)#1. **3**: Cg(2) = O(2) O(2)#1 N(3); Cg(3) = O(4) O(5) N(4). **4**: Cg(5) = O(1) O(4) N(4); Cg(6) = O(2) O(5) N(3). **5**: Cg(4) = O(2) O(4) N(3); Cg(5) = O(2) N(4) N(5).

843

844

845

846

847

848

849

850

851 **Table 2**. Detailed parameters extracted from the photophysical properties of 1–5a

852

Sample	$\lambda_{max\text{-}abs}$ (log(ε))	λ_{exc}	$\lambda_{max\text{-}em}$	Φ_s
1	200 (4.75), 276 (4.62)	229	344	0.99[b]
2	204 (4.78), 256 (4.56), 274 (4.53)		337	0.057[b]
3	203 (5.34), 279 (5.12)		345	0.13[b]
4	205 (4.97), 269 (4.96)		346	0.069[b]
5	203 (5.27), 281 (4.95), 320 (4.43)	320	355	0.65[c]

[a] All the wavelengths are given in nm. ε values are given in M^{-1} cm^{-1}. $\lambda_{max\text{-}abs}$ = maximum of absorption; λ_{exc} = excitation maximum; $\lambda_{max\text{-}em}$ = maximum of emission; Φ_s = quantum yield samples. [b] Relative quantum yield values using L-tyrosine as the standard (Φ = 0.14).[66] [c] Relative quantum yield values using quinine sulphate as the standard (Φ = 0.577).[67]

853

854

855

856

857

858

859

860

Table 3. Crystal data and structure refinement for 1–3

	1	2	3
Empirical formula	$C_{27}H_{25}CdN_3O_6$	$C_{44}H_{46}CdN_4O_{10}$	$C_{66}H_{64}Cd_2N_8O_{14}$
Formula weight	599.90	903.25	1418.05
T (K)	100(2)	100(2)	100(2)
Wavelength (Å)	0.71073	0.71073	0.71073
System, space group	Monoclinic, $P2_1/n$	Monoclinic, $P2_1/c$	Triclinic, $P\bar{1}$
Unit cell dimensions			
a (Å)	14.2599(5)	8.5444(3)	9.1064(7)
b (Å)	10.0971(4)	22.0061(8)	12.4497(10)
c (Å)	17.8998(6)	11.1259(4)	14.1999(12)
α (°)	90	90	101.718(3)
β (°)	103.0770(10)	98.9050(10)	106.897(3)
γ (°)	90	90	90.206(3)
V (Å^3)	2510.44(16)	2066.77(13)	1504.9(2)
Z	4	2	1
D_{calc} (mg m^{-3})	1.587	1.451	1.565
μ (mm^{-1})	0.918	0.592	0.782
F(000)	1216	932	724
Crystal size (mm^{-3})	0.150 × 0.140 × 0.080	0.180 × 0.140 × 0.060	0.180 × 0.040 × 0.020
hkl ranges	$-20 \le h \le 20$, $-14 \le k \le 14$, $-25 \le l \le 25$	$-12 \le h \le 9$, $-31 \le k \le 31$, $-15 \le l \le 15$	$-13 \le h \le 13$, $-18 \le k \le 18$, $-20 \le l \le 20$
θ range (°)	2.331 to 30.527	2.584 to 30.530	2.343 to 31.596
Reflections collected/unique/[R_{int}]	40 461/7615/0.0371	44 074/6266/0.0295	56 350/10 043/0.0434
Completeness to θ (%)	99.6	99.4	99.8
Absorption correction	Semi-empirical from equivalents	Semi-empirical from equivalents	Semi-empirical from equivalents
Max. and min. transmission	0.7461 and 0.6583	0.7461 and 0.6718	0.7463 and 0.6966
Refinement method	Full-matrix least-squares on $\|F\|^2$	Full-matrix least-squares on $\|F\|^2$	Full-matrix least-squares on $\|F\|^2$
Data/restrains/parameters	7615/0/340	6266/6/281	10 043/6/416
Goodness-on-fit on $\|F\|^2$	1.101	1.054	1.060
Final R indices [$I > 2\sigma(I)$]	R_1 = 0.0262, wR_2 = 0.0530	R_1 = 0.0232, wR_2 = 0.0566	R_1 = 0.0315, wR_2 = 0.0750
R indices (all data)	R_1 = 0.0387, wR_2 = 0.0626	R_1 = 0.0285, wR_2 = 0.0614	R_1 = 0.0391, wR_2 = 0.0803
Extinction coefficient	n/a	n/a	n/a
Largest diff-peak and hole (e Å^{-3})	0.872 and −0.632	0.442 and −0.516	1.020 and −1.029

871 **Table 4**. Crystal data and structure refinement for 4 and 5

872

	4	5
Empirical formula	$C_{40}H_{46}CdN_4O_9$	$C_{43}H_{45}CdN_7O_8$
Formula weight	839.21	900.26
T (K)	100(2)	100(2)
Wavelength (Å)	0.71073	0.71073
System, space group	Monoclinic, $P2_1/c$	Triclinic, $P\bar{1}$
Unit cell dimensions		
a (Å)	15.1674(4)	11.8826(7)
b (Å)	16.9696(4)	13.1721(9)
c (Å)	15.2451(4)	13.5190(10)
α (°)	90	78.902(3)
β (°)	98.5900(10)	88.255(3)
γ (°)	90	83.346(2)
V (Å^3)	3879.84(17)	2062.3(2)
Z	4	2
D_{calc} (mg m^{-3})	1.437	1.450
μ (mm^{-1})	0.623	0.592
F(000)	1736	928
Crystal size (mm^{-3})	0.200 × 0.150 × 0.060	0.080 × 0.045 × 0.040
hkl ranges	$-21 \le h \le 21$, $-24 \le k \le 24$, $-21 \le l \le 21$	$-16 \le h \le 16$, $-18 \le k \le 18$, $-19 \le l \le 19$
θ range (°)	2.136 to 30.527	2.300 to 30.563
Reflections collected/unique/[R_{int}]	41 832/11696/0.0363	93 667/12 616/0.0447
Completeness to θ (%)	99.4	99.8
Absorption correction	Semi-empirical from equivalents	Semi-empirical from equivalents
Max. and min. transmission	0.7461 and 0.6641	0.7461 and 0.6861
Refinement method	Full-matrix least-squares on $\|F\|^2$	Full-matrix least-squares on $\|F\|^2$
Data/restrains/parameters	11 696/2/494	12 616/3/605
Goodness-on-fit on $\|F\|^2$	1.063	1.055
Final R indices [$I > 2\sigma(I)$]	R_1 = 0.0336, wR_2 = 0.0726	R_1 = 0.0400, wR_2 = 0.1002
R indices (all data)	R_1 = 0.0479, wR_2 = 0.0828	R_1 = 0.0518, wR_2 = 0.1109
Extinction coefficient	n/a	n/a
Largest diff-peak and hole (e Å^{-3})	1.521 and −1.130	1.130 and −1.174

873

874

875

876

877

878

879

880

Figures Captions

Scheme 1. Outline of the synthesis of complexes 1–5.

Figure 1. (a) Molecular structure of 1. (b) Detailed view of the intramolecular interactions of each polymeric chain. (c) General view of the (220) plane. (d) Detailed view of the intermolecular interactions between adjacent chains.

Figure. 2 (a) Molecular structure of 2 with its intramolecular interactions assigned. General view of the supramolecular expansions along the (b) ac plane and (c) [011] direction.

Figure 3. (a) Molecular structure of 3. (b) Detailed view of the intramolecular interactions. General view of: (c) a-directed supramolecular chain and (d) bc supramolecular plane.

Figure 4. (a) Molecular structure of 4. (b) General view of the supramolecular bc plane. (c and d) Detailed views of the intermolecular interactions

Figure 5. (a) Molecular structure of 5. (b) General view of the ab plane. (c) Detailed view of the N–H···O synthon and C–H···O intermolecular interactions forming the ab plane. (d) General view of the chain formed along the [$1\bar{1}1$] direction

Figure 6. Representation of the geometry of the Cd(II) cores in (a) 1, (b) 2, (c) 3, (d) 4, and (e) 5.

Figure 7. Orientation of the methyl groups and the aromatic rings of dPy in complexes (a) 1, (b) 2, (c) 3, (d) 4 and (e) 5.

Figure 8. Emission spectra of complexes 1–5 excited at their corresponding excitation maxima (229 nm (1–4) and 320 nm (5)) in MeOH solution (1.00 × 10−7 M).

Scheme 1.

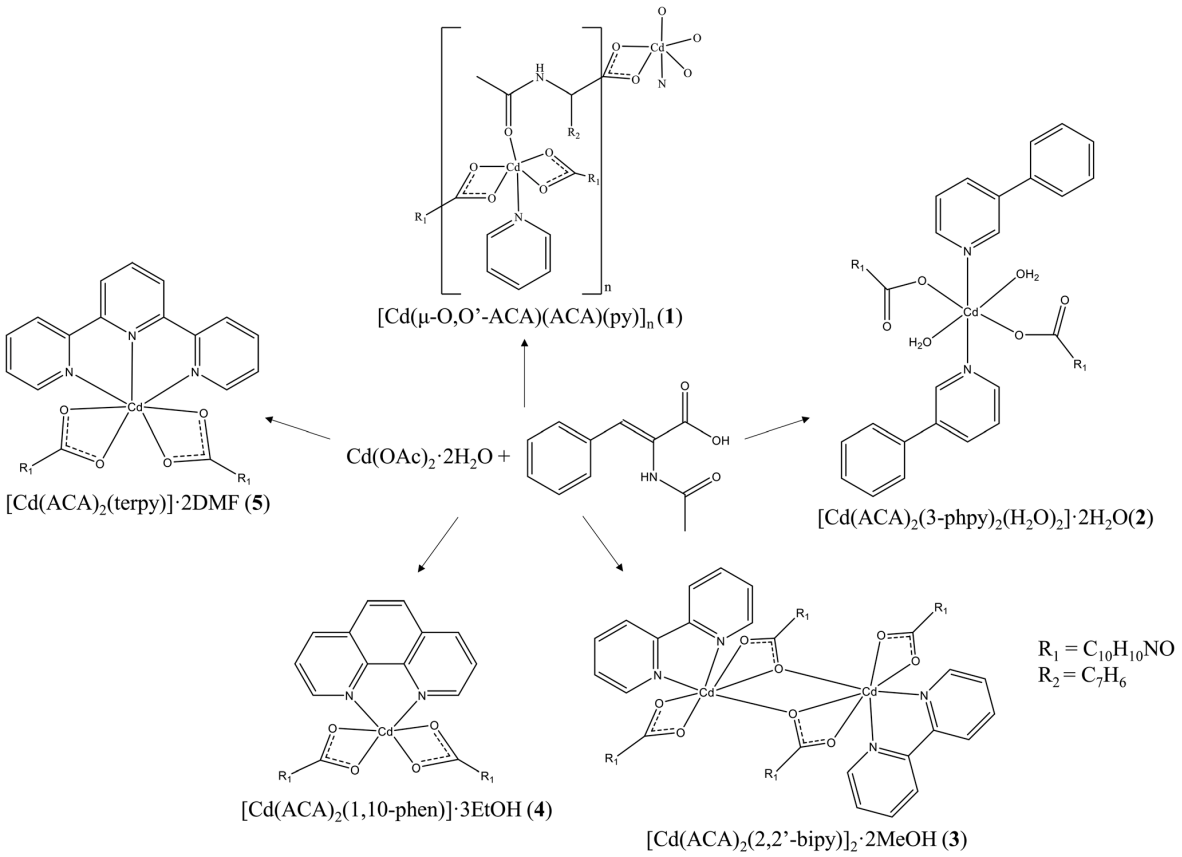
[Cd(μ-O,O'-ACA)(ACA)(py)]n (1)
Cd(OAc)2·2H2O +
[Cd(ACA)2(terpy)]·2DMF (5)
[Cd(ACA)2(3-phpy)2(H2O)2]·2H2O(2)
[Cd(ACA)2(1,10-phen)]·3EtOH (4)
[Cd(ACA)2(2,2'-bipy)]2·2MeOH (3)
R1 = C10H10NO
R2 = C7H6

Figure 1

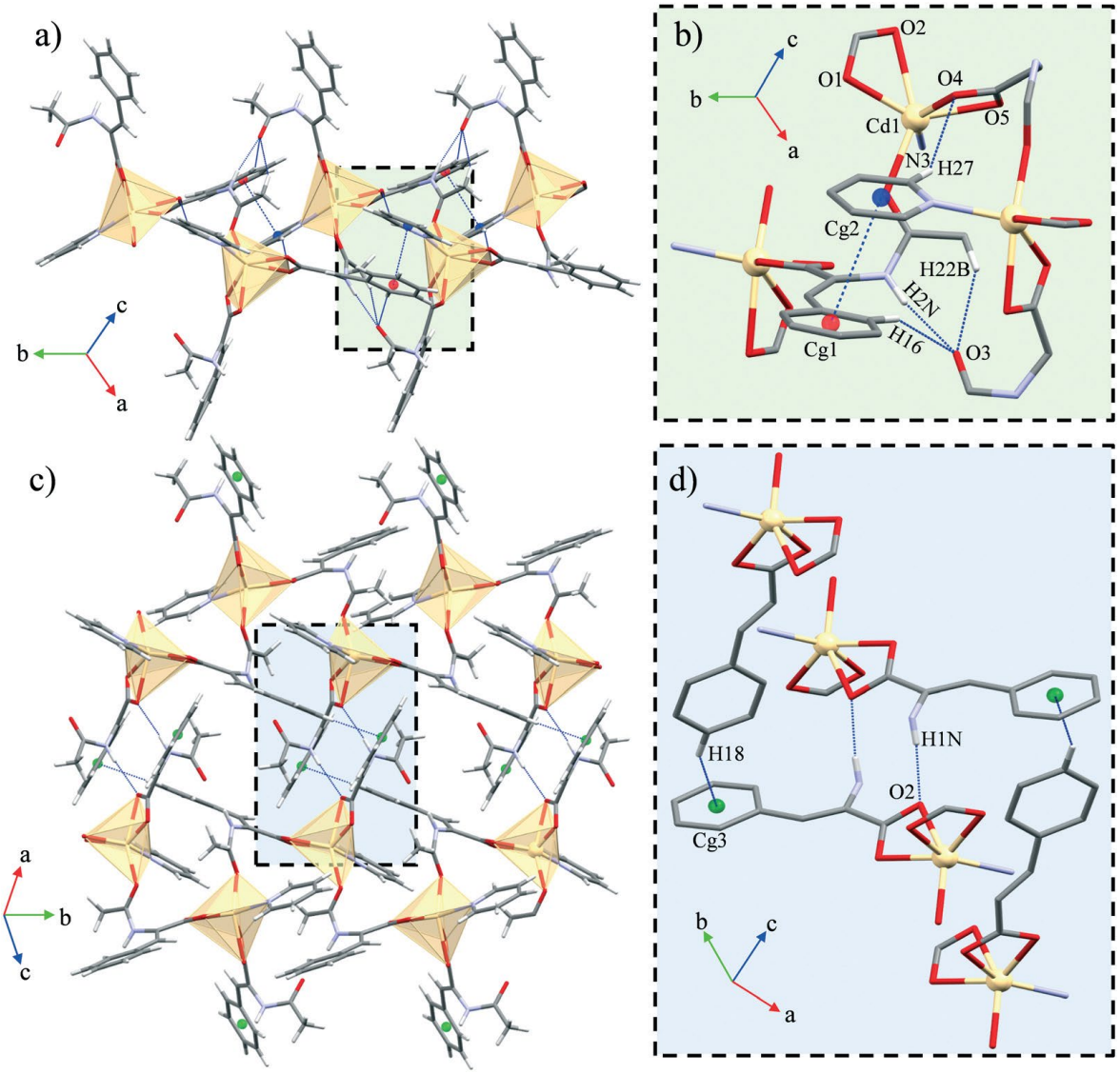
a)
c
b
a
b)
c
b
a
O2
O1
O4
Cd1
O5
N3
H27
Cg2
H22B
H2N
Cg1
H16
O3
c)
a
b
c
d)
H18
H1N
O2
Cg3
b
c
a

Figure 2

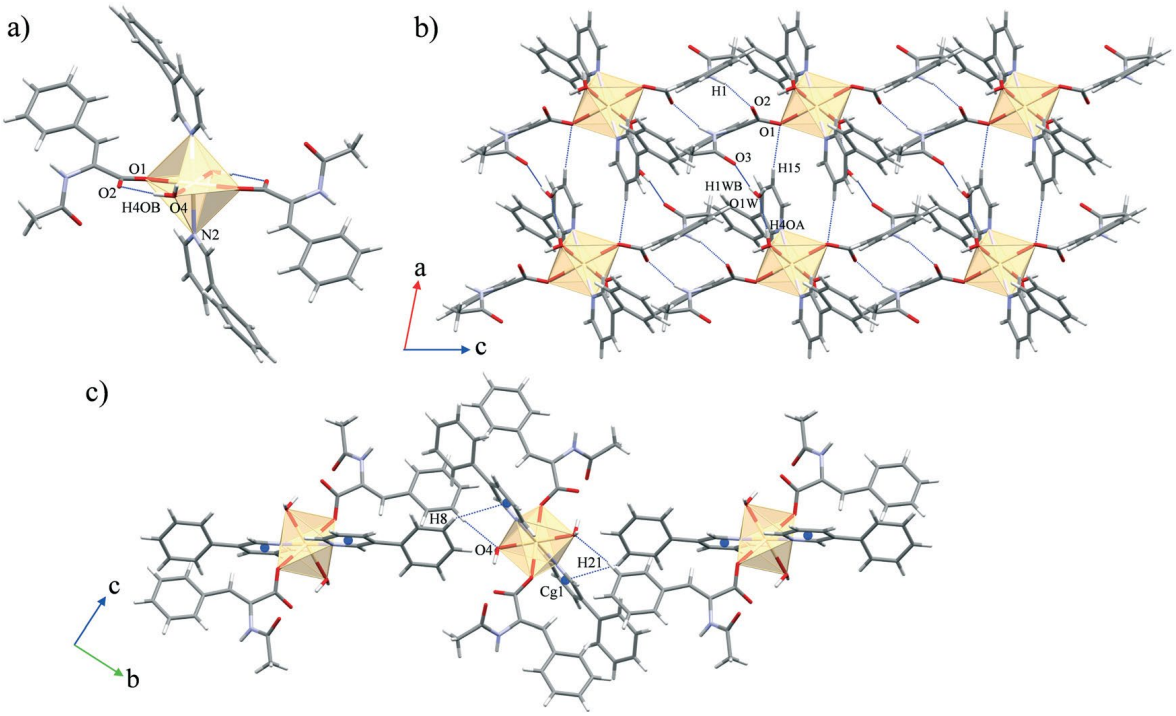
a)
O1
O2
H4OB
O4
N2
b)
H1
O2
O1
O3
H15
H1WB
O1W
H4OA
a
c
c)
H8
O4
H21
Cg1
c
b

Figure 3

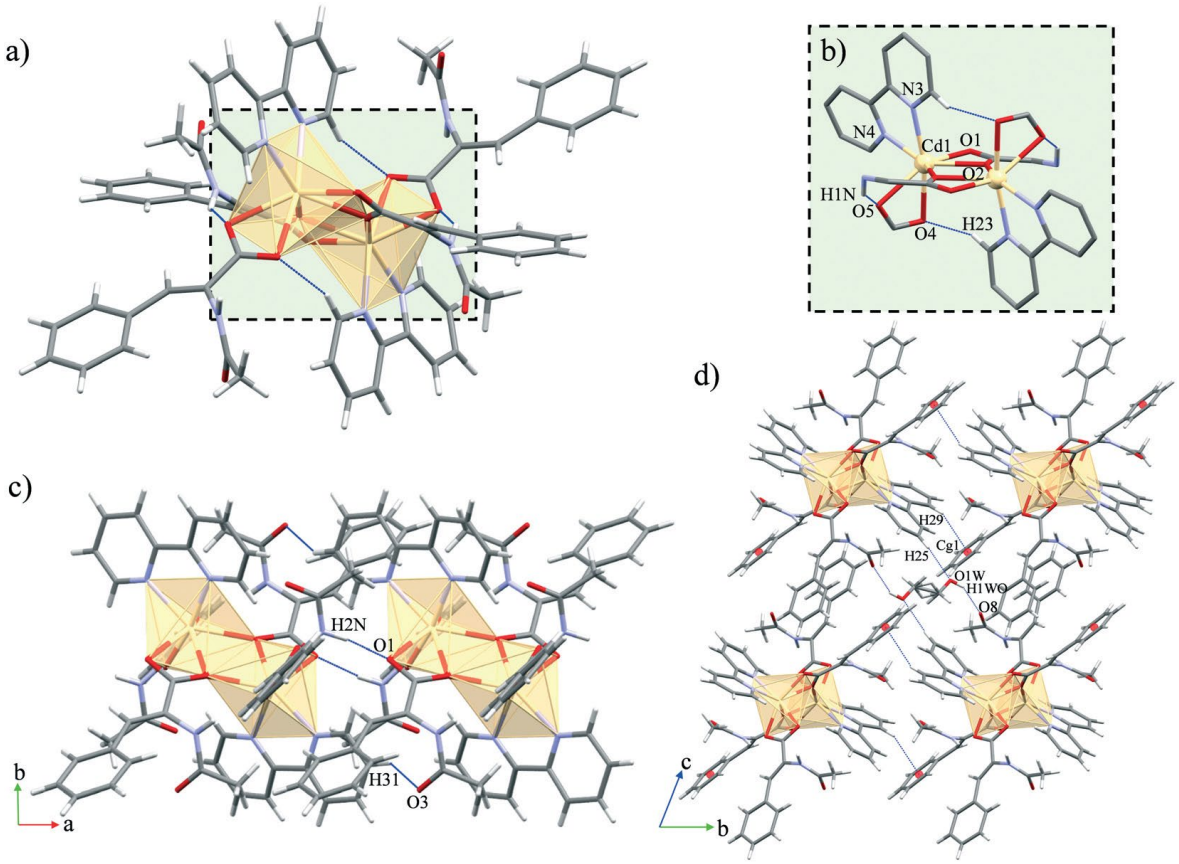
a)
b)
N3
N4
Cd1
O1
O2
H1N
O5
O4
H23
c)
H2N
O1
H31
O3
b
a
d)
H29
Cg1
H25
O1W
H1WO
O8
c
b

Figure 4

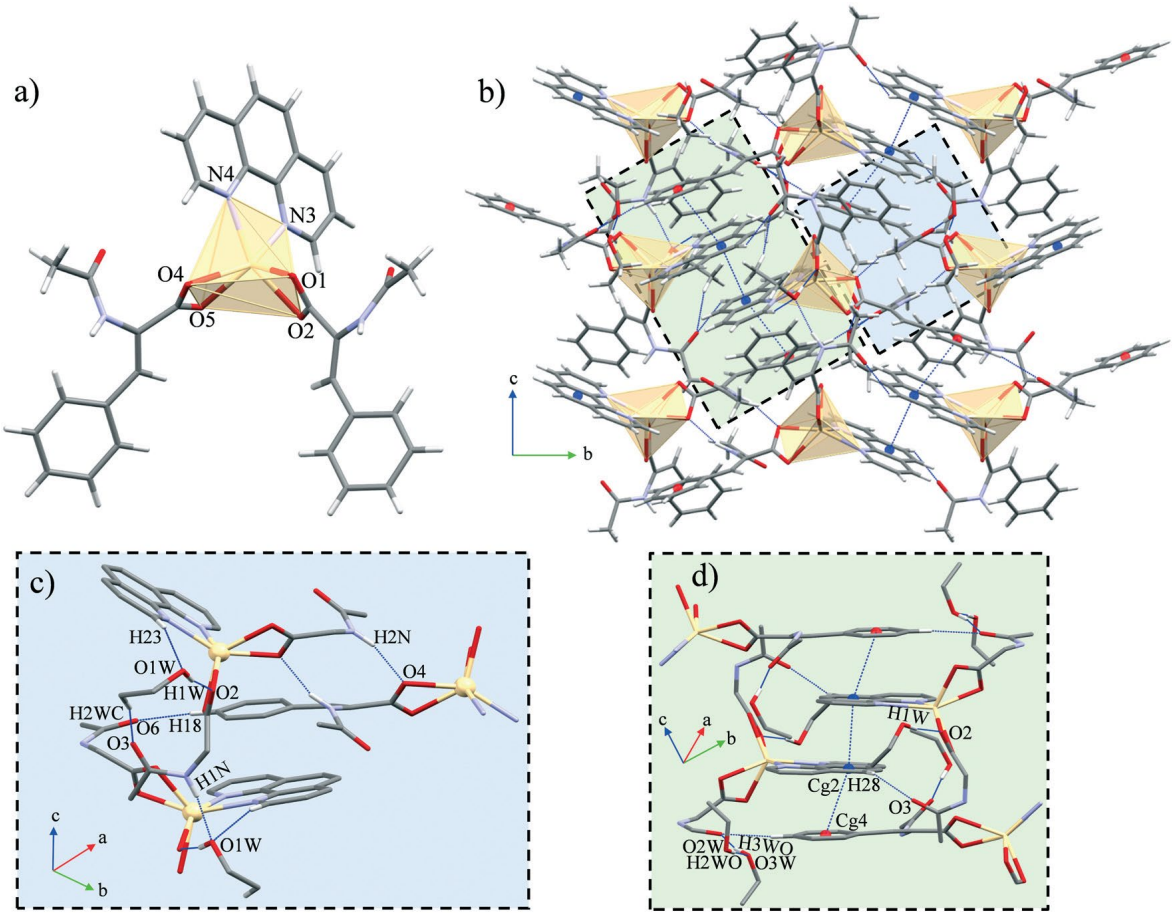
a)
N4
N3
O4
O1
O5
O2
b)
c
b
c)
H23
O1W
H1W
O2
H2WC
O6
H18
O3
H1N
O1W
H2N
O4
c
a
b
d)
H1W
O2
c
a
b
Cg2
H28
O3
Cg4
O2W
H3WO
H2WO
O3W

Figure 5

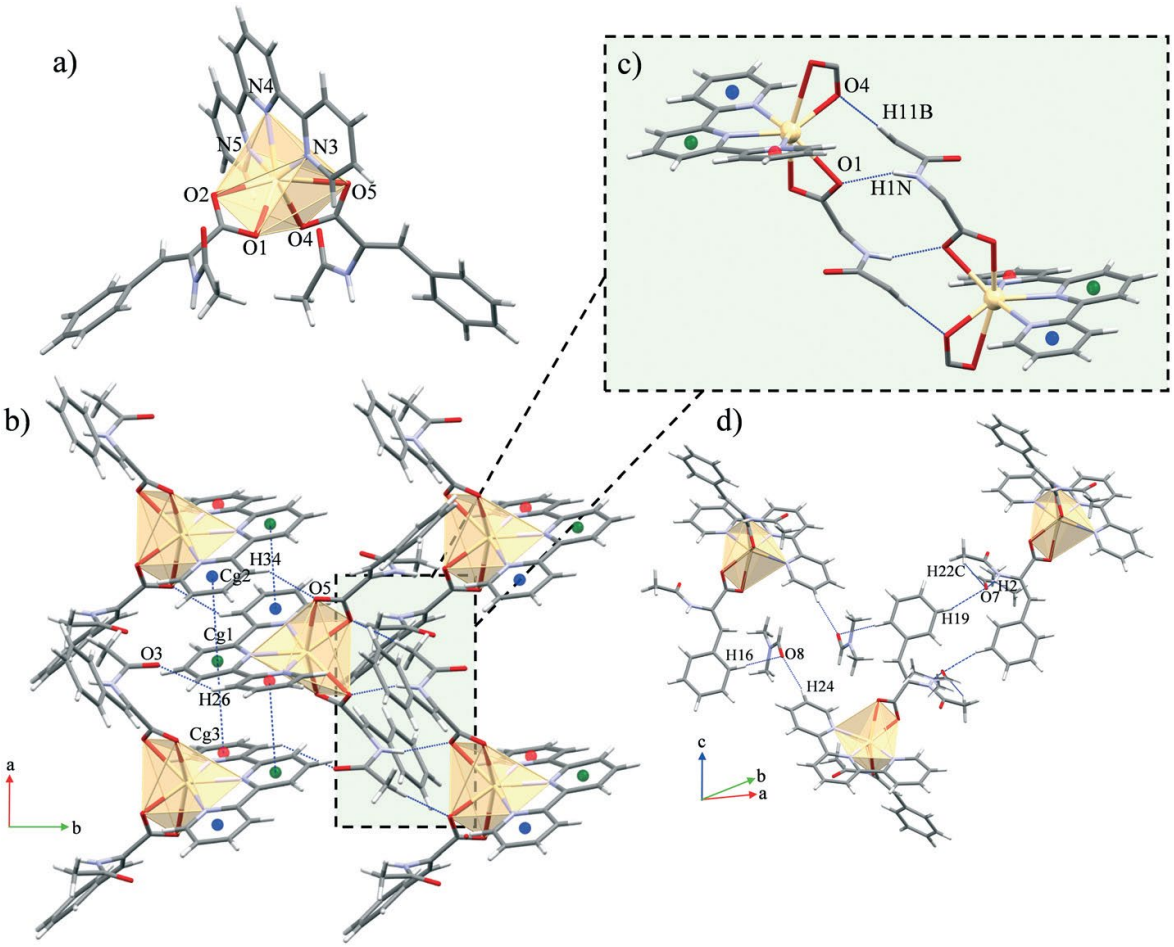
a)
N4
N5
N3
O2
O5
O1
O4
b)
H34
Cg2
O5
Cg1
O3
H26
Cg3
a
b
c)
O4
H11B
O1
H1N
d)
H22C
O7
H2
H19
H16
O8
H24
c
b
a

Figure 6

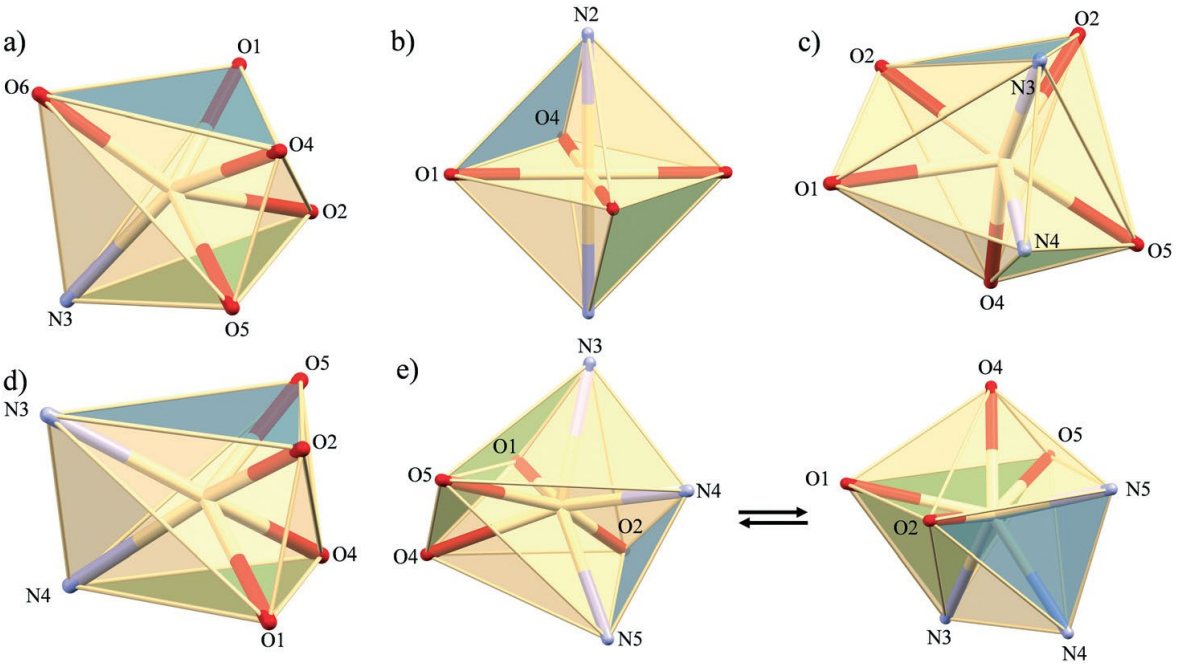
a)
O1
O6
O4
O2
N3
O5
b)
N2
O4
O1
c)
O2
O2
N3
O1
N4
O5
O4
d)
O5
N3
O2
O4
N4
O1
e)
N3
O1
O5
N4
O2
O4
N5
O4
O5
O1
N5
O2
N3
N4

977 **Figure 7**

978

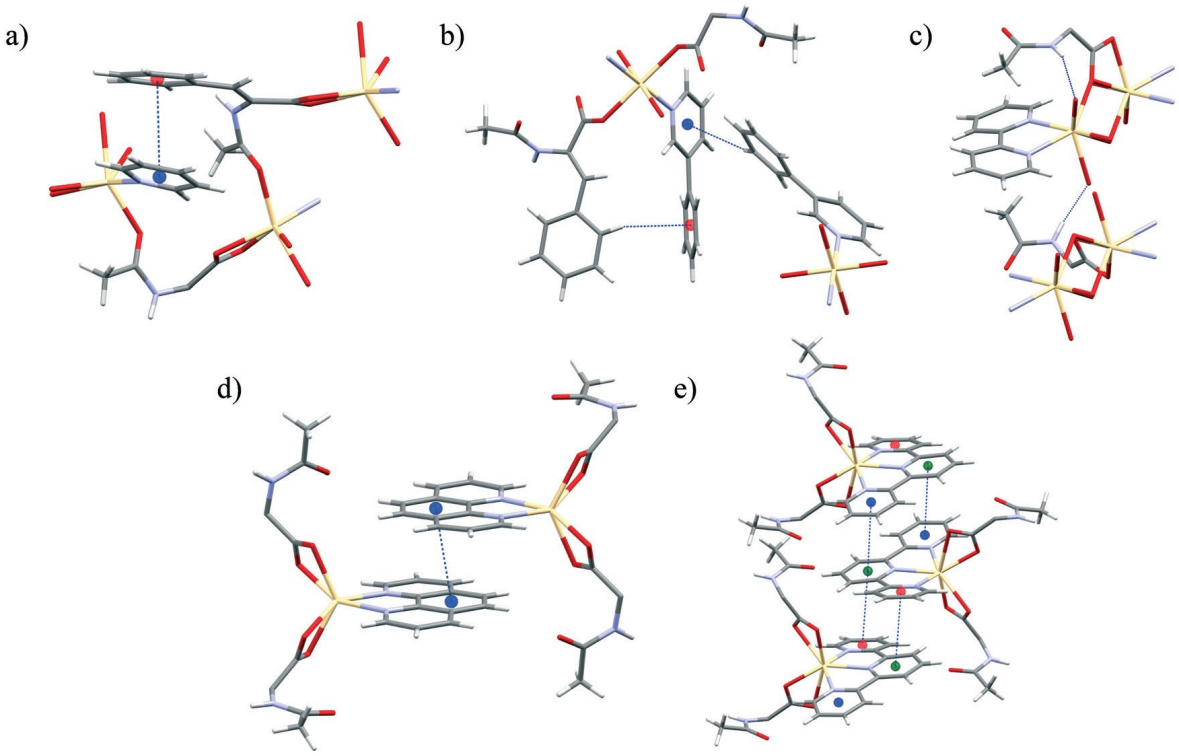

979

980

981

982

983

984

985 **Figure 8**

986

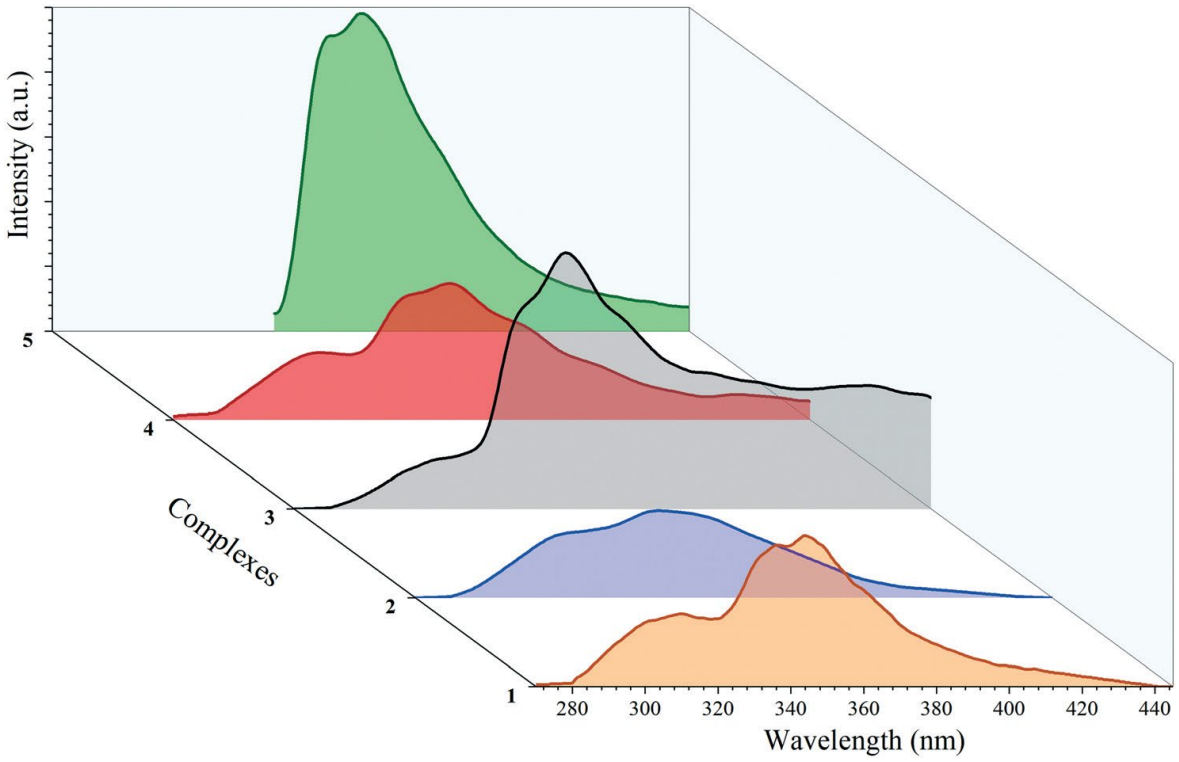

987

988

989

990

991

992